Adipocyte Metabolic Pathways Regulated by Diet Control the Female Germline Stem Cell Lineage in *Drosophila melanogaster*

Shinya Matsuoka, Alissa R. Armstrong,[1] Leesa L. Sampson,[2] Kaitlin M. Laws,[3] and Daniela Drummond-Barbosa[4]

Department of Biochemistry and Molecular Biology, Johns Hopkins University, Bloomberg School of Public Health, Baltimore, Maryland

ABSTRACT Nutrients affect adult stem cells through complex mechanisms involving multiple organs. Adipocytes are highly sensitive to diet and have key metabolic roles, and obesity increases the risk for many cancers. How diet-regulated adipocyte metabolic pathways influence normal stem cell lineages, however, remains unclear. *Drosophila melanogaster* has highly conserved adipocyte metabolism and a well-characterized female germline stem cell (GSC) lineage response to diet. Here, we conducted an isobaric tags for relative and absolute quantification (iTRAQ) proteomic analysis to identify diet-regulated adipocyte metabolic pathways that control the female GSC lineage. On a rich (relative to poor) diet, adipocyte Hexokinase-C and metabolic enzymes involved in pyruvate/acetyl-CoA production are upregulated, promoting a shift of glucose metabolism toward macromolecule biosynthesis. Adipocyte-specific knockdown shows that these enzymes support early GSC progeny survival. Further, enzymes catalyzing fatty acid oxidation and phosphatidylethanolamine synthesis in adipocytes promote GSC maintenance, whereas lipid and iron transport from adipocytes controls vitellogenesis and GSC number, respectively. These results show a functional relationship between specific metabolic pathways in adipocytes and distinct processes in the GSC lineage, suggesting the adipocyte metabolism–stem cell link as an important area of investigation in other stem cell systems.

KEYWORDS stem cells; adipocytes; metabolism; germline; oogenesis; *Drosophila*

ADULT stem cell lineages function within multicellular organisms subject to variable nutrient availability, and dynamic physiology and metabolic state. Stem cells and their progeny can sense and respond to physiological changes through many diet-dependent pathways in organisms ranging from invertebrates to mammals (Ables *et al.* 2012). There is also a link between intrinsic metabolic changes and the decision between self-renewal and differentiation in stem cell lineages (Shyh-Chang *et al.* 2013; Chandel *et al.* 2016). Much less is known about how metabolic pathways in one tissue influence adult stem cell lineages in a distinct tissue.

Adipocytes are highly sensitive to diet and play major metabolic and endocrine roles. Adipocytes contribute to energy homeostasis by storing and mobilizing lipids, and they produce proteohormones, or adipokines, that modulate many physiological processes, including insulin sensitivity, appetite, and reproduction (Rosen and Spiegelman 2014; Fasshauer and Bluher 2015). Obesity, which often leads to adipocyte dysfunction, leads to increased risk for a number of diseases, including many types of cancers (Deng *et al.* 2016). However, how metabolic pathways within adipocytes might influence stem cell lineages in other established adult tissues remains a largely open question.

The *Drosophila melanogaster* female germline stem cell (GSC) lineage is responsive to diet (Ables *et al.* 2012). At the anterior of each ovariole, the germarium houses two to three GSCs that are readily identifiable in a well-defined niche composed mainly of

doi: https://doi.org/10.1534/genetics.117.201921
Manuscript received March 8, 2017; accepted for publication April 5, 2017; published Early Online April 7, 2017.
Supplemental material is available online at www.genetics.org/lookup/suppl/doi:10.1534/genetics.117.201921/-/DC1.
[1]Present address: Department of Biological Sciences, University of South Carolina, Columbia, SC 29208.
[2]Present address: Vanderbilt Center for Stem Cell Biology, Vanderbilt University, Nashville, TN 37232.
[3]Present address: Department of Neuroscience, University of Pennsylvania, Philadelphia, PA 19104.
[4]Corresponding author: John Hopkins University, 615 North Wolfe St., Room W3118, Baltimore, MD 21205. E-mail: dbarbosa@jhu.edu

cap cells (Figure 1, A and B). Each GSC division yields a GSC and a cystoblast that divides to generate a 16-cell cyst. Follicle cells envelop the cyst, giving rise to an egg chamber, or follicle, that develops through fourteen stages to form a mature oocyte (Figure 1B) (Spradling 1993). GSCs and their progeny grow and divide faster on yeast-rich relative to -poor diets, and the survival of early germline cysts and vitellogenic follicles is reduced on a poor diet (Drummond-Barbosa and Spradling 2001). Multiple diet-dependent factors, including insulin-like peptides, the steroid ecdysone, the nutrient sensor Target of Rapamycin (TOR), AMP-dependent kinase, and the adiponectin receptor, mediate this response (Ables *et al.* 2012; Laws *et al.* 2015; Laws and Drummond-Barbosa 2016).

Adipocyte factors contribute to the GSC lineage response to diet. In *Drosophila*, adipocytes are present in close association with hepatocyte-like oenocytes in an organ called the fat body (Figure 1A) (Gutierrez *et al.* 2007; Arrese and Soulages 2010; Chatterjee *et al.* 2014). Adipocytes make up the bulk of the fat body mass that underlies the cuticle and surrounds major organs, and have evolutionarily conserved metabolic pathways (Kühnlein 2012). Adipocyte-specific disruption of amino acid transport causes GSC loss and a partial block in ovulation via the GCN2 kinase and TOR, respectively (Armstrong *et al.* 2014), indicating that adipocytes communicate their nutritional status to the ovary. Nevertheless, the mixture of nutrients in the *Drosophila* yeast-based diet includes far more than just amino acids, presumably leading to an equally complex response of adipocytes with potential consequences to other tissues. How diet affects adipocyte metabolic pathways, and whether or not such pathways might have roles in regulating the ovary, has remained unclear.

In this study, to identify adipocyte metabolic pathways that respond quickly to diet and contribute to the regulation of the GSC lineage, we used an isobaric tags for relative and absolute quantification (iTRAQ) proteomic approach to compare the fat body proteomes of females on yeast-rich or -poor diets. Of a total of 2525 proteins identified, 450 proteins were significantly up- or downregulated within 12 hr of switching from rich to poor diets. Of these 450 diet-regulated proteins, 80 were predicted metabolic enzymes (including regulatory enzymes) in 55 distinct metabolic pathways. Our bioinformatics analysis of these proteomic data suggests that there is a metabolic shift in glycolysis within adipocytes to support the biosynthesis of sugars, nucleic acids, and fatty acids on a rich diet. In adipocytes of females on a rich (relative to poor) diet, enzymes in the citric acid cycle and electron transport chain are downregulated, whereas Hexokinase-C (Hex-C) and Phosphoenolpyruvate carboxykinase (Pepck) (both of which contribute to pyruvate production), and enzymes involved in the production of acetyl-CoA are upregulated, presumably to support macromolecule biosynthesis. Through adult adipocyte-specific knockdown of key metabolic enzymes, we uncovered a functional relationship between Hex-C and other enzymes involved in pyruvate/acetyl-CoA production in adipocytes, and the survival of early germline cysts. Enzymes catalyzing fatty acid oxidation and phosphatidylethanolamine (PE) synthesis are also upregulated in adipocytes on a rich diet, and these enzymes promote GSC maintenance. Finally, carrier proteins involved in the transport of lipids and iron are also regulated by diet in adipocytes, and they control vitellogenesis and GSC number, respectively. Taken together, these data reveal specific effects of adipocyte metabolism on the GSC lineage, providing new insight into the connection between adipocytes and tissue stem cell lineages.

Materials and Methods

Drosophila strains and culture conditions

Fly stocks were maintained at 22–25° on standard medium containing cornmeal, molasses, yeast, and agar. We used standard medium supplemented with wet yeast paste as a rich diet and medium containing only molasses and agar without wet yeast paste as a poor diet, as described (Armstrong *et al.* 2014). *yw* was used as a wild-type strain for the iTRAQ proteomic analysis. GFP/Venus trap lines for *ATPCL* (*ATPCL^{CB04427}*) and *CG4825* (*CG4825^{CPTI003911}*) were obtained from A. Spradling (Buszczak *et al.* 2007) and the Kyoto *Drosophila* Genomics and Genetic Resources/Kyoto Stock Center (DGGR#115456) (Lowe *et al.* 2014). *tub-Gal80^{ts}*; *3.1 Lsp2-Gal4* (*Lsp2^{ts}*) was used as an adult adipocyte-specific Gal4 driver (Armstrong *et al.* 2014). The following *UAS-hairpin RNA* lines [for RNA interference (RNAi)] from the Vienna *Drosophila* RNAi Stock Center (VDRC) and the Transgenic RNAi Project collection at Bloomington *Drosophila* Stock Center (BDSC) were used: *luc^{JF01355}* (BDSC#31603); *Hex-C^{GD12378}* (VDRC#35337); *Pepck^{GD16827}*(*Pepck RNAi #1*, VDRC#50253); *Pepck^{GD9451}* (*Pepck RNAi #2*, VDRC#20529); *ATPCL^{GD3552}* (VDRC#30282); *AcCoAS^{HMS02314}* (BDSC#41917); *CG3961^{GD2713}* (*CG3961 RNAi #1*, VDRC#37305); *CG3961^{KK102693}* (*CG3961 RNAi #2*, VDRC#107281); *eas^{GD10683}* (*eas RNAi #1*, VDRC#34287); *eas^{KK102681}* (*eas RNAi #2*, VDRC#103784); *CG4825^{GD2753}* (VDRC#5391); *Fer1HCH^{GD4853}* (*Fer1HCH RNAi #1*, VDRC#12925); *Fer1HCH^{GD16271}* (VDRC#49536); *Lpp^{GD3156}* (*Lpp RNAi #1*, VDRC#6878); *Lpp^{HMS00265}* (*Lpp RNAi #2*, BDSC#33388); and *Lpp^{HM05157}* (*Lpp RNAi #3*, BDSC#28946). Randomly selected *KK* lines (*CG44402^{KK109637}*, *CG4236^{KK102930}*, *CG3630^{KK108188}*, and *CG4143^{KK109070}*) that possess RNAi transgenes in an annotated extra pKC43 landing site and cause dominant phenotypes when crossed with *elav-Gal4* (Green *et al.* 2014) also showed severe GSC-loss phenotypes when crossed with *Lsp2^{ts}*. To avoid the potential dominant GSC-loss phenotypes of *KK* lines (which may contain an insertion in the extra pKC43 landing site) driven by *Lsp2^{ts}*, we examined landing site occupancy using a previously described PCR-based method (Green *et al.* 2014). Only *KK* lines with RNAi transgenes inserted exclusively in the nonannotated pKC43 landing site were used.

Adult adipocyte-specific RNAi

For adult adipocyte-specific RNAi induction, we used the previously characterized adipocyte-specific Gal4 (*3.1 Lsp2-Gal4*)

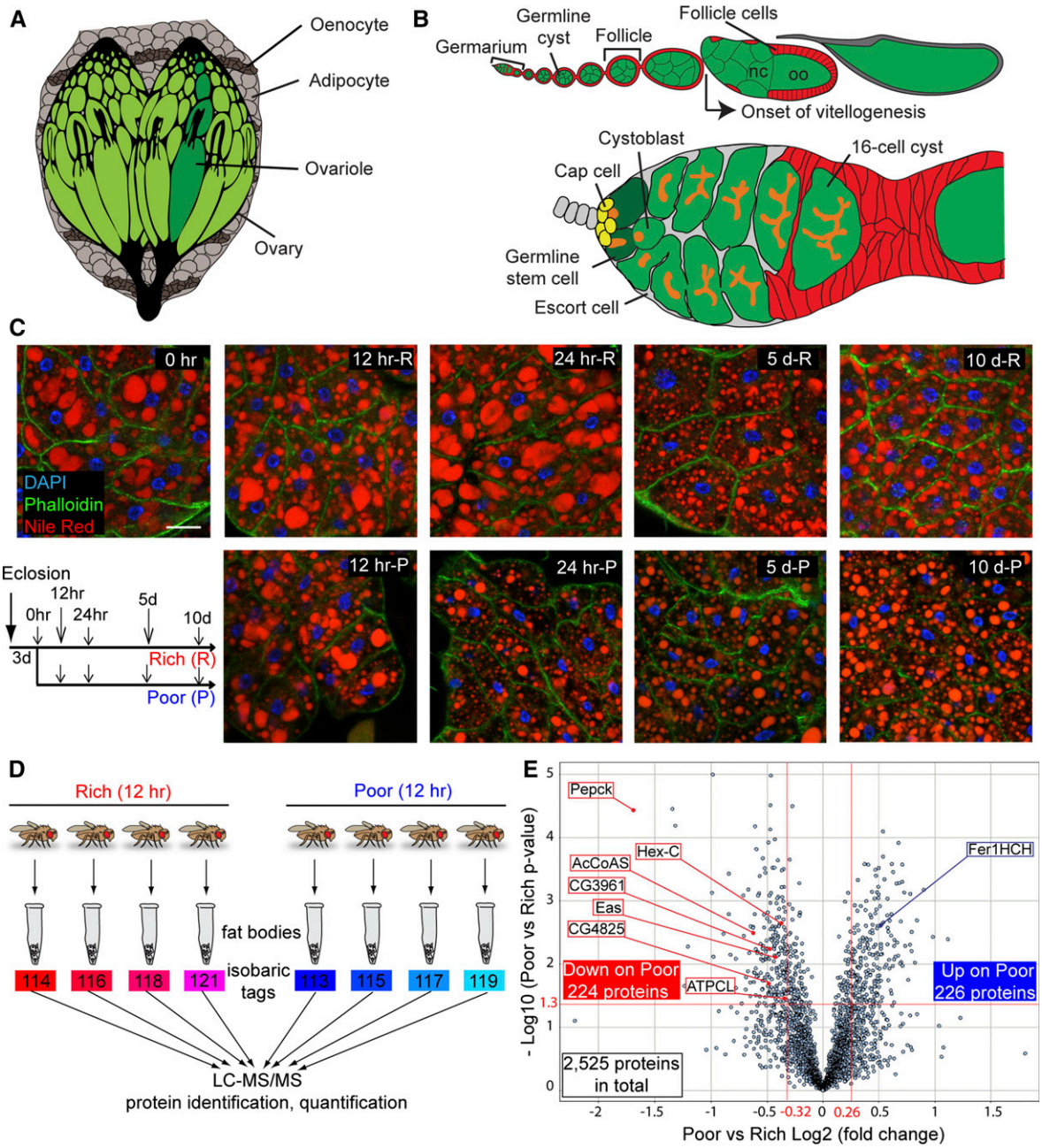

Figure 1 The fat body proteome undergoes significant changes within 12 hr of dietary switch. (A) The *Drosophila* fat body, composed of adipocytes and hepatocyte-like oenocytes, surrounds multiple organs. (B) Structure of ovariole (top) and germarium (bottom). Each ovariole contains chronologically arranged follicles, each composed of a 16-cell germline cyst (one oocyte, oo, and 15 nurse cells, nc) enveloped by follicle cells, and vitellogenesis begins at stage 8. Follicles are formed in the germarium, which contains germline stem cells (GSCs) associated with cap cells and a subset of escort cells. Each GSC division produces one GSC and one cystoblast that incompletely divides four times to form a 16-cell cyst. A germline-specific organelle, the fusome (orange), becomes progressively more branched as cysts divide. (C) Adipocyte morphology on different diets. Newly eclosed females were kept for 3 days on a rich diet (R) prior to being switched to a poor diet (P). Control females remained on a rich diet. DAPI (blue), adipocyte nuclei; Nile Red (red), lipid droplets; Phalloidin (green), cell membranes. Scale bar, 40 μm. (D) Isobaric tags for relative and absolute quantification (iTRAQ) flow chart. Four replicates of fat body proteins from females maintained for 12 hr on either rich or poor diets were subjected to iTRAQ analysis. LC-MS/MS, liquid chromatography - tandem mass spectrometry. (E) Volcano plot showing fat body proteins identified by iTRAQ. Proteins with Poor *vs.* Rich ratio < 0.8 or > 1.2 (red lines at -0.32 and 0.26, respectively, on *x*-axis) and showing a *P*-value of < 0.05 by Student's *t*-test (red line at 1.3 on *y*-axis) were considered differentially expressed in response to diet. The *x*-axis values represent Log2 (Poor to Rich fold change), whereas *y*-axis values represent $-$Log10 (Poor *vs.* Rich *P*-value). Eight differentially expressed proteins analyzed in this study are indicated. AcCoAS, acetyl-CoA synthase; ATPCL, ATP citrate lyase; CG3961, long-chain acyl-CoA synthase; CG4825, phosphatidylserine synthase 1; Eas, Ethanolamine kinase; Fer1HCH, Ferritin 1 Heavy Chain Homolog; Hex-C, hexokinase-C; Pepck, phosphoenolpyruvate carboxykinase.

in conjunction with the temperature-sensitive ubiquitously expressed Gal80 (*tub-Gal80^{ts}*) transgene (Armstrong *et al.* 2014). Females of genotypes *tub-Gal80^{ts}/UAS-RNAi*; *3.1 Lsp2-Gal4/+* or *tub-Gal80^{ts}/+*; *3.1 Lsp2-Gal4/UAS-RNAi* (where *UAS-RNAi* represents different hairpin transgenes used in this study) were raised at 18° (the permissive temperature for Gal80^{ts}) (McGuire *et al.* 2003) to prevent RNAi induction during development. After eclosion, 0–2-day-old females were maintained at 18° for 3 days with *yw* males on a rich diet, then switched to 29° (the restrictive temperature for Gal80^{ts}) for various lengths of time to induce adult adipocyte-specific RNAi.

Egg counts

Five pairs of flies (females of appropriate genotype and *yw* males) were maintained in perforated plastic bottles with molasses/agar plates covered by a thin layer of wet yeast paste at 29° in triplicate. Plates were changed every 24 hr, and eggs produced within 24 hr at 5 days of RNAi induction were counted and the average number of eggs produced per female calculated. Data were subjected to Student's *t*-test.

Ovary immunostaining and fluorescence microscopy

Ovaries were dissected in Grace's medium (Bio Whittaker) and fixed for 13 min in 5.3% formaldehyde (Ted Pella) in Grace's medium at room temperature. Ovaries were subsequently rinsed and washed three times for 15 min in PBT [0.1% Triton X-100 (Sigma) in phosphate-buffered saline (PBS)] and blocked for 3 hr in blocking solution [5% normal goat serum (NGS, Jackson ImmunoResearch) and 5% bovine serum albumin (BSA, Sigma) in PBT]. Ovaries were then incubated overnight at 4° in the following primary antibodies diluted in blocking solution: mouse monoclonal anti-Hts (1B1) (DSHB, 1:10); mouse anti-α-Spectrin (3A9) (DSHB, 1:50); mouse anti-Lamin C (LC28.26) (DSHB, 1:50); and rabbit anti-cleaved Dcp1 (Cell Signaling Technology, #9578; 1:200). Ovaries were rinsed and washed three times for 15 min in PBT and then incubated at room temperature for 2 hr in Alexa Fluor 488- or 568-conjugated secondary antibodies (Molecular Probes) diluted in blocking solution (1:200). Ovaries were rinsed and washed three times for 15 min in PBT and mounted in Vectashield with DAPI (Vector Laboratories). When ovaries were stained with anti-α-Spectrin antibody, 0.1% Tween 20 (Sigma) in PBS instead of 0.1% Triton X-100 in PBS was used for all steps. EdU (5-ethynyl-2′-deoxyuridine) incorporation (Life Technologies) was carried out as described (Armstrong *et al.* 2014). Images were collected with a Zeiss LSM700 confocal microscope or a Zeiss AxioImager-A2 fluorescence microscope.

Quantification of GSC number, GSC proliferation, early germline cyst death, and vitellogenic egg chamber death

GSCs were identified based on their juxtaposition to cap cells (visualized by Lamin C) and spectrosome morphology and position (visualized by Hts or α-Spectrin), as described (Laws and Drummond-Barbosa 2015). Rates of GSC loss over time were calculated using two-way ANOVA with interaction (GraphPad Prism 6), as described (Armstrong *et al.* 2014). As a measure of GSC proliferation, the fraction of EdU-positive GSCs was calculated as a percentage of the total number of GSCs analyzed. Early germline cyst death in germaria was measured based on the fraction of germaria containing cleaved Dcp1-positive germ cells or germ cells with pyknotic nuclei (visualized by DAPI as highly condensed DNA) as a percentage of the total number of germaria analyzed. Follicles at vitellogenic stages (stage 8 and beyond) were identified based on size and morphology (Spradling 1993). Dying vitellogenic follicles were readily recognizable by the presence of pyknotic nuclei, as described (Armstrong *et al.* 2014), and the fraction of ovarioles with dying vitellogenic follicles was calculated as a percentage of the total number of ovarioles analyzed, as described (Laws and Drummond-Barbosa 2015). Data for GSC proliferation, early germline cyst death, and vitellogenic follicle death were subjected to χ^2 analysis.

Visualization and quantification of lipid droplets, and nuclear and cell sizes in adipocytes

To visualize lipid droplets in adipocytes, Nile Red dye (Sigma) was used. Dissected fat bodies with abdominal carcasses were fixed in 5.3% formaldehyde (Ted Pella) in Grace's medium for 20 min at room temperature, and rinsed and washed three times for 15 min in PBT. Fat bodies with abdominal carcasses were then incubated with Alexa Fluor 488-conjugated Phalloidin (1:200, Molecular Probes) in PBT for 20 min, and rinsed and washed three times for 15 min in PBT. Fat bodies with abdominal carcasses were stored in 50% glycerol in PBS containing 0.5 μg/ml DAPI and 25 ng/ml Nile Red dye. Fat bodies were scraped off abdominal carcass before mounting and imaging in a Zeiss LSM700 confocal microscope.

To measure adipocyte nuclear diameter, largest nuclear diameters (visualized by DAPI) were selected and measured using ImageJ. To measure adipocyte area, largest cell areas were selected (based on Phalloidin staining) and measured using ImageJ. To quantify total lipid volume in adipocytes, the diameters of all lipid droplets (visualized by Nile Red) in each adipocyte were first measured by ImageJ. The volume of each lipid droplet was then calculated using the equation $(4\pi r^3)/3$ (r: radius). The volumes of all lipid droplets in each adipocyte were added to calculate its total lipid volume. Data were subjected to Student's *t*-test.

Adipocyte tetramethylrhodamine, ethyl ester (TMRE) and Mito Tracker Green FM (MTGFM) staining

To measure adipocyte mitochondrial activity, freshly dissected fat bodies were scraped off abdominal cuticles in Grace's medium kept at room temperature and subsequently incubated with Grace's medium containing 50 nM TMRE (Sigma), a membrane potential-dependent dye, and 400 nM MTGFM (Thermo Fisher Scientific), a membrane potential-independent dye, for 20 min at room temperature. Both TMRE and MTGFM have been previously used in *Drosophila* fat body and S2 cells (Baron *et al.* 2016; Barry and Thummel 2016). Fat bodies were

then rinsed three times and mounted in Grace's medium and images were taken using Zeiss LSM700 confocal microscope. Using ImageJ, background-subtracted total TMRE and MTGFM intensities were measured, and the TMRE value (corresponding to total mitochondrial activity) was divided by the MTGFM value (corresponding to total mitochondrial mass) to calculate normalized adipocyte mitochondrial activity levels. Data were subjected to Student's *t*-test.

iTRAQ labeling and strong cation exchange fractionation

Zero–3-day-old *yw* females were collected and maintained on a rich diet with *yw* males for 3 days and either maintained on a rich diet or switched to a poor diet for 12 hr. Abdominal fat bodies were then manually scraped off the cuticles from either 60 flies on a rich diet or 90 flies switched to a poor diet in quadruplicate. Fat bodies were subsequently placed in an equal volume of 2 × NuPAGE LDS Sample Buffer (Thermo Fisher Scientific) and brought up to 45 μl volume by adding additional 1 × NuPAGE LDS Sample Buffer. Next, 5 μl of NuPAGE Sample Reducing Agent (Thermo Fisher Scientific) were added. Fat body protein samples were homogenized, boiled for 10 min, and centrifuged at 13,200 rpm for 2 min. Protein amounts were quantified by EZQ Protein Quantification Kit (Thermo Fisher Scientific). Fat body protein samples were diluted, TCA (trichloroacetic acid)/acetone precipitated such that each contained 83 μg of fat body proteins, and resuspended in 20 μl 500 mM TEAB (triethyl ammonium bicarbonate) and 1 μl 2% SDS. Each sample was reduced by adding 2 μl 50 mM TCEP [tris-(2-carboxyethyl) phosphine] for 1 hr at 60°, alkylated by 1 μl 200 mM MMTS (methyl methanethiosuphonate) for 15 min at room temperature, then digested at 37° overnight with trypsin (Promega, sequencing grade, www.promega.com) using a 1:10 enzyme to protein ratio. Samples were labeled by adding 100 μl of an iTRAQ reagent (dissolved in isopropanol) and incubating at room temperature for 2 hr. All samples were dried to a volume of ~30 μl and subsequently mixed. The combined peptide sample was diluted to 8 ml of strong cation exchange (SCX) loading buffer (25% v/v acetonitrile and 10 mM KH_2PO_4, pH 2.8) and subsequently fractionated by SCX chromatography on an Agilent 1200 Capillary HPLC system using a PolySulfoethyl A column (2.1 × 100 mm, 5 μm, 300 Å, PolyLC; polylc.com). The sample was loaded and washed isocratically with 25% v/v acetonitrile and 10 mM KH_2PO_4, pH 2.8 for 40 min at 250 μl/min. Peptides were eluted and collected in 1 min fractions using a 0–350 mM KCl gradient in 25% v/v acetonitrile and 10 mM KH_2PO_4, pH 2.8, over 40 min at 250 μl/min, monitoring elution at 214 nm. The SCX fractions were dried, resuspended in 200 μl 0.05% TFA (trifluoroacetic acid), and desalted using an Oasis HLB μElution plate (Waters Associates, www.waters.com).

Mass spectrometry (MS) analysis

Desalted peptides were loaded for 15 min at 750 nl/min directly on to a 75 μm × 10 cm column packed with Magic C18 (5 μm, 120 Å, Michrom Bioresources, www.michrom.com). Peptides were eluted using a 5–40% B (90% acetonitrile in 0.1% formic acid) gradient over 90 min at 300 nl/min. Eluting peptides were sprayed directly into an LTQ Orbitrap Velos mass spectrometer (Thermo Fisher Scientific, www.thermo.com/orbitrap) through a 1 μm emitter tip (New Objective, www.newobjective.com) at 1.6 kV. Survey scans (full MS) were acquired from 350 to 1800 m/z with up to 10 peptide masses (precursor ions) individually isolated with a 1.2 Da window and fragmented (MS/MS) using a collision energy of 45 and 30 sec dynamic exclusion. Precursor and fragment ions were analyzed at 30,000 and 7500 resolution, respectively.

The MS/MS spectra were extracted and searched against the *D. melanogaster* database from the Reference Sequence (RefSeq) 40 database using Mascot (Matrix Science) through Proteome Discoverer software (v1.2, Thermo Fisher Scientific) specifying the sample's species, trypsin as the enzyme allowing one missed cleavage, fixed cysteine methylthiolation and 8-plex-iTRAQ labeling of N-termini, and variable methionine oxidation and 8-plex-iTRAQ labeling of lysine and tyrosine. Peptide identifications from Mascot searches were processed within the Proteome Discoverer to identify peptides with a confidence threshold 1% False Discovery Rate (FDR), based on a concatenated decoy database search. A protein's ratio is the median ratio of all unique peptides identifying the protein at a 1% FDR. Technical variation was < 20%, as empirically determined from an eight-sample technical replicate 8-plex iTRAQ experiment.

The iTRAQ MS spectra data were exported from Proteome Discoverer v1.4 (Thermo Fisher Scientific) software and imported into Partek Genomics Suite v6.6 (Partek) for further analysis. MS data underwent normalization to minimize the technical differences between iTRAQ lanes and illuminate differential protein concentrations between the four replicates each of Poor and Rich samples. To ensure unambiguous nomenclature and ease of evaluation, all spectra's protein GenInfo (GI) identifiers were mapped to their cognate genes in the NCBI Entrez database (gene symbols are used in this study) and both identifiers are included in all tables. All peptide spectra first underwent quality control (QC) for Proteome Discoverer Isolation Interference values < 30% and passing values were transformed to log2 notation. For each sample, all spectra's median log2 signal values were determined for each peptide and deemed to represent that peptide, yielding one value per each of the resulting 2525 peptides per sample. These median signal values were then quantile normalized to minimize potential differences across the eight iTRAQ lanes. A one-way ANOVA, using Partek's *t*-test, evaluated each protein's relative concentration as fold change between the Poor and Rich classes and determined the statistical significance of that difference in terms of its *P*-value. These values were then exported for further evaluation and graphical representation to Spotfire DecisionSite with Functional Genomics v9.1.2 (TIBCO Spotfire, Boston, MA).

Gene ontology (GO) term and pathway analyses

To determine enriched GO terms for total fat body proteins identified by iTRAQ, DAVID Bioinformatics Database (https://david.ncifcrf.gov) (Huang da *et al.* 2009) and GOrilla (http://cbl-gorilla.cs.technion.ac.il/) (Eden *et al.* 2009) were used. The 2525 proteins identified were compared to all proteins encoded in the *Drosophila* genome. To determine enriched GO terms for fat body proteins down- or upregulated on a poor diet, 224 down- and 226 upregulated proteins on a poor diet were compared to 2525 total proteins identified by iTRAQ using DAVD Bioinformatics Database. We used the KEGG (Kyoto Encyclopedia of Genes and Genomes) PATHWAY Database (http://www.genome.jp/kegg/pathway.html) (Kanehisa *et al.* 2016) to determine the metabolic pathways in which enzymes down- or upregulated on a poor diet are involved.

Western blotting

To extract fat body protein, fat bodies from at least 15 flies were scraped off abdominal cuticles in Grace's medium and transferred to a tube containing 20 μl of RIPA (radioimmunoprecipitation assay) buffer [50 mM Tris-HCl pH 6.8, 150 mM NaCl, 1 mM EDTA, 0.5% deoxycholate, 1% NP-40 (nonyl phenoxypolyethoxylethanol), and cOmplete Mini, EDTA-free (Roche)]. Samples were vortexed for 3 min at 4° and centrifuged at 13,200 rpm for 5 min at 4°. Next, 5 μl of supernatant were collected to determine protein amounts by Pierce BCA Protein Assay Kit (Thermo Fisher Scientific), and the remaining 15 μl of each supernatant were brought up to 20 μl by NuPAGE LDS sample buffer (Life Technologies) containing 5% β-mercaptoethanol (Sigma), boiled at 70° for 10 min, and stored at −20° before SDS-PAGE. To collect hemolymph proteins, antennae were manually removed from 40 flies and the hemolymph coming out of the antennal regions was collected by centrifugation (~1 μl hemolymph can be collected from 40 flies); this method was modified from previously published hemolymph extraction protocols (MacMillan and Hughson 2014; Tennessen *et al.* 2014). No cells were present in extracted hemolymph based on Hoechst 33342 staining. Next, 19 μl PBS were added and samples for BCA assay and SDS-PAGE were prepared as described above. Approximately 15–20 μg of protein per sample were loaded for SDS-PAGE. The following antibodies were used for Western blotting: rabbit anti-GFP (Torrey Pines, 1:5000); rat anti-Hex-C (1:4000) (Kim *et al.* 2008); rabbit anti-Eas (1:2000) (Pascual *et al.* 2005); mouse anti-Fer1HCH (1:2000) (Tang and Zhou 2013a); and HRP-conjugated anti-rabbit, rat, and mouse IgG (GE Healthcare, 1:50,000). The chemiluminescent signal was developed by either SuperSignal West Pico or SuperSignal West Femto (Thermo Fisher Scientific). Band intensity was quantified using ImageJ by subtracting background pixels from band pixels in a fixed size box and normalized to the background-subtracted total proteins visualized by MemCode Reversible Protein Stain Kit (Thermo Fisher Scientific). Controls were set to one and experimental band intensities were determined relative to control. Each experiment was carried out twice and representative images were shown.

Triglyceride (TAG) assay

Fat bodies with abdominal carcasses from 10 females were dissected in Grace's medium and homogenized in 70 μl PBT [0.05% Tween 20 (Sigma) in PBS]. Samples were then centrifuged at 13,200 rpm for 5 min at 4°. 5 μl of supernatants were collected to determine protein amounts by Pierce BCA Protein Assay Kit (Thermo Fisher Scientific), and 50 μl of supernatants were boiled at 70° for 10 min and stored at −80°. TAG amounts were determined by Serum Triglyceride Determination Kit (Sigma) according to the manufacturer's protocol. TAG amounts were normalized to protein amounts and expressed by μg TAG/μg protein. Data were subjected to Student's *t*-test.

RT-PCR

Fat bodies from 2 to 10 females at 7 days of RNAi induction were manually dissected in RNAlater solution (Ambion). RNA was then extracted by the RNAqueous-4PCR DNA-free RNA isolation for RT-PCR kit (Ambion) according to the manufacturer's protocol. Primers used were as follows: *Rp49* forward (5′-CAGTCGGATCGATATGCTAAGC-3′); *Rp49* reverse (5′-AATCTCCTTGCGCTTCTTGG-3′); *Lpp* forward (5′-TATTGATGG CATACGCACC-3′); and *Lpp* reverse (5′-ACAATGGACTTCT GAGCCT-3′). Band intensity was quantified using Axio Vision by subtracting background pixels from band pixels in a fixed size box and normalized to that of the *Rp49* band. Control was set to one and experimental band intensities were determined relative to control value.

Data availability

Drosophila strains are available upon request. All data generated for this study are included in the main text and figures or in the supplemental materials provided.

Results

Proteins involved in metabolism are enriched in the adult female fat body proteome

To identify adipocyte metabolic pathways that respond relatively fast to diet, we performed a quantitative proteomic comparison between hand-dissected fat bodies from females on yeast-rich or -poor diets using iTRAQ analysis (Ross *et al.* 2004). Lineage tracing experiments had shown that changes in oogenesis rates are detected within 18 hr of switching between rich and poor diets (Drummond-Barbosa and Spradling 2001), indicating that key regulatory events occur earlier. We also examined the adipocytes in females on a rich diet or switched to a poor diet for different lengths of time. At 12 hr, there were no obvious changes in adipocyte morphology or lipid content, despite a small decrease in cell size (Figure 1C and Supplemental Material, Figure S1 in File S1). In contrast, at 24 hr, the number and volume of lipid

A

Enriched GO terms for total fat body proteins	Number of proteins (Total encoded)	*P-value*	Benjamini
GO:0008152 Metabolic process	1319 (4580)	3.72E-55	7.81E-54
GO:0051179 Localization	490 (1718)	1.44E-11	7.53E-11
GO:0016043 Cellular component organization	495 (1768)	2.74E-10	1.15E-09
GO:0022610 Biological adhesion	56 (188)	0.015234	0.04501

B

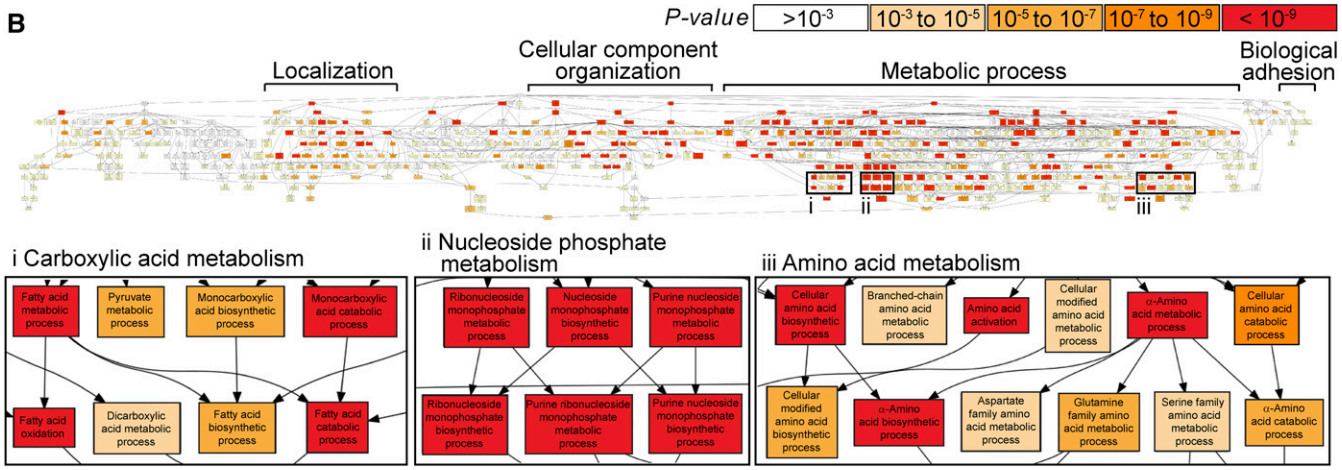

Figure 2 The fat body proteome is enriched for metabolic proteins. (A) Gene ontology (GO) term analysis of fat body proteome using DAVID. The number of proteins identified by iTRAQ (isobaric tags for relative and absolute quantification) in each GO category is listed. The total number of proteins encoded in the *Drosophila* genome in each category is shown in parentheses. The original *P*-value and corrected *P*-value (Benjamini) are shown (Fisher's exact test). (B) Visual representation of GO term analysis of fat body proteome using GOrilla (Eden *et al.* 2009). Proteins involved in metabolic processes are highly enriched.

droplets decreased, resulting in a marked drop in stored lipids (Figure 1C and Figure S1, A–C in File S1). Over longer periods of time, lipid content decreased in both diets (Figure 1C and Figure S1, A–C in File S1); we speculate that the relentless demand from high rates of oogenesis contributes to the time-dependent decrease in stored lipids on a rich diet. Nuclear condensation, a known nuclear response to starvation (Moraes *et al.* 2005; Parker *et al.* 2007), was observed on a poor diet at 5 and 10 days (Figure 1C and Figure S1E in File S1). Therefore, we performed our iTRAQ analysis at the 12-hr time point, to focus on primary changes in adipocyte protein levels in response to diet.

For the iTRAQ analysis, we cultured newly eclosed females on a rich diet for 3 days, then either maintained them on a rich diet or switched them to a poor diet for 12 hr (Figure 1D). We hand-dissected the female fat bodies and subjected the extracted protein samples to iTRAQ proteomic analysis, which reproducibly identified 2525 proteins (Figure 1, D and E and Table S1). GO term analysis using DAVID and GOrilla bioinformatics tools (Eden *et al.* 2009; Huang da *et al.* 2009) revealed that 52% of those proteins are involved in metabolic processes (Figure 2A). This enrichment in proteins related to metabolism in the fat body is consistent with its known metabolic functions (Arrese and Soulages 2010). Among enriched metabolic pathways were those in the metabolism of carboxylic acids, nucleoside phosphates, and amino acids (Figure 2B). Proteins that regulate the localization of a protein complex or organelle (19%), cellular component organization such as assembly or disassembly of organelles (19%), and biological adhesion (2%) were also enriched in fat bodies (Figure 2A). The highly metabolic nature of the fat body was therefore captured by our proteomic approach.

Expression levels of 80 metabolic enzymes change rapidly in the fat body in response to diet

Of the 2525 proteins identified, 224 were downregulated and 226 were upregulated within 12 hr on a poor diet (Figure 1E and Table S2 and Table S3). Proteins involved in translation and metabolism were downregulated (Figure 3A), pointing to a reduction in overall protein synthesis and metabolism. Adhesion and actomyosin structure proteins were upregulated (Figure 3B), suggesting that cytoskeletal remodeling might accompany cell size changes on a poor diet (Figure 1C and Figure S1D in File S1).

The fat body is highly specialized for metabolism (Figure 2) and many of its metabolic proteins respond to diet (Figure 3A). To test if diet-regulated proteins in adipocytes might modulate oogenesis, we focused on metabolic enzymes and categorized them into distinct pathways using the KEGG PATHWAY Database (Kanehisa *et al.* 2016). The levels of 80 predicted metabolic enzymes spanning 55 distinct metabolic pathways that control the production of lipids, amino acids, nucleic acids, and carbohydrates were regulated by diet (Figure 3C and Table S4). Importantly, 33 of those are regulatory enzymes that catalyze irreversible steps of metabolic reactions (Table S4), thereby helping

A

Enriched GO terms for fat body proteins downregulated on a poor diet	Number of proteins (Total identified)	*P-value*	Benjamini
GO:0006412 Translation	40 (208)	1.39E-05	0.013278
GO:0008152 Metabolic process	145 (1319)	4.10E-03	0.071482
GO:0034645 Cellular macromolecule biosynthetic process	45 (284)	4.81E-04	0.142788
GO:0044249 Cellular biosynthetic process	65 (459)	4.18E-04	0.181868

B

Enriched GO terms for fat body proteins upregulated on a poor diet	Number of proteins (Total identified)	*P-value*	Benjamini
GO:0007155 Cell adhesion	21 (55)	1.06E-08	1.18E-05
GO:0048856 Anatomical structure development	53 (312)	8.24E-07	3.05E-04
GO:0032502 Developmental process	63 (422)	5.11E-06	9.45E-04
GO:0032989 Cellular component morphogenesis	21 (104)	5.36E-04	0.044782
GO:0031032 Actomyosin structure organization	7 (15)	0.001151	0.087284
GO:0007517 Muscle organ development	10 (36)	0.00322	0.189888

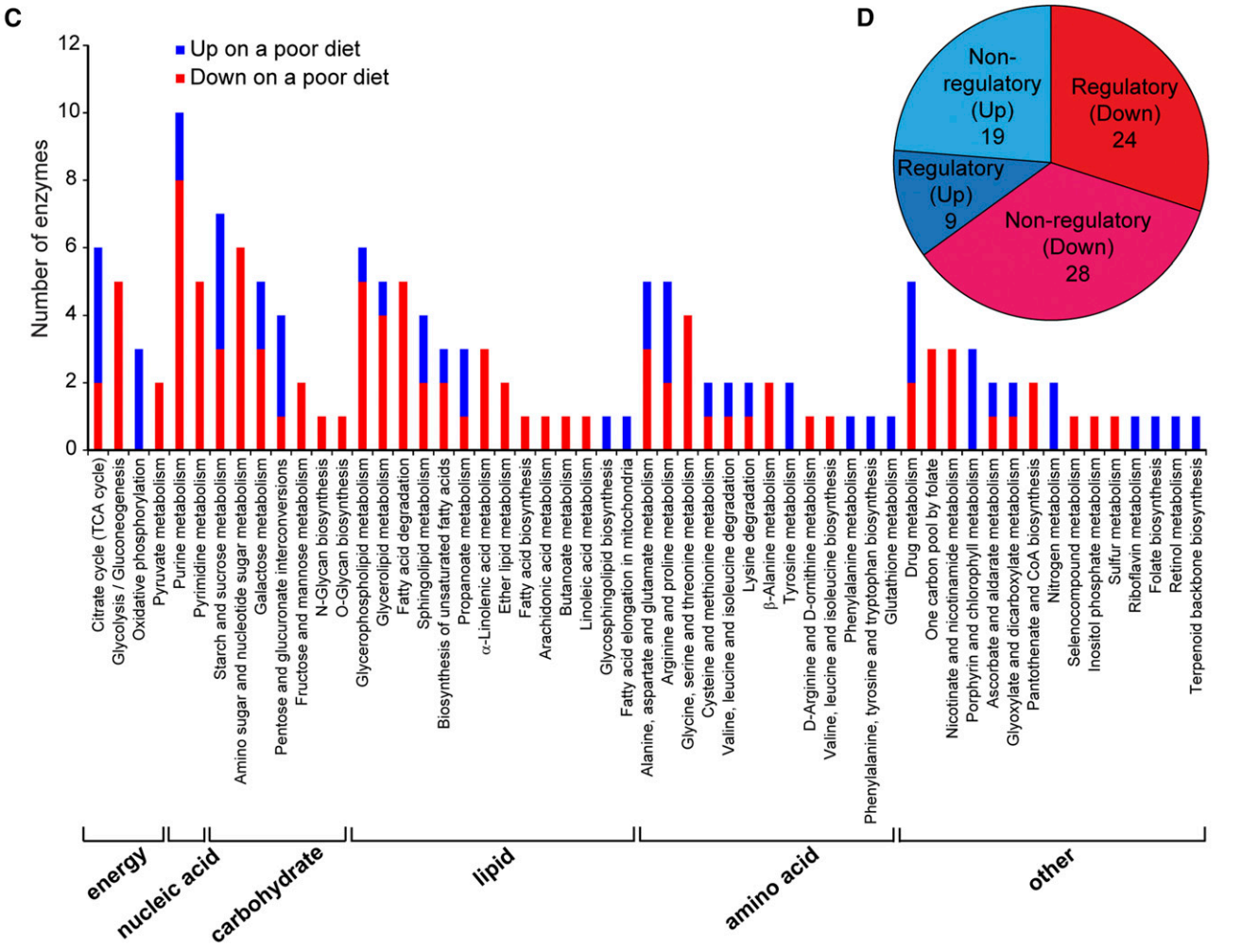

Figure 3 Eighty metabolic enzymes including 33 regulatory enzymes are differentially expressed in response to diet. (A and B) GO term analysis of fat body proteins downregulated (A) or upregulated (B) on a poor diet using DAVID. The number of proteins downregulated or upregulated on a poor diet is shown for each GO category. The total number of proteins identified in the fat body proteome for each category is shown in parentheses. The original *P*-value and corrected *P*-value (Benjamini) are shown (Fisher's exact test). (C) Distribution of 80 metabolic enzymes downregulated or upregulated on a poor diet spanning 55 metabolic pathways using KEGG. A subset of metabolic enzymes maps to two or more metabolic pathways that partially overlap, such that the sum of metabolic enzymes plotted in the graph is > 80. (D) Pie chart of metabolic enzymes downregulated or upregulated on a poor diet. Among 145 proteins with the GO term "metabolic process" downregulated on a poor diet (A), only 52 (24 regulatory plus 28 nonregulatory) represent metabolic enzymes. GO, Gene ontology; KEGG, Kyoto Encyclopedia of Genes and Genomes; TCA, tricarboxylic acid.

to determine the amount of metabolites produced (Figure 3D and Figure S2 in File S1).

The fat body on a rich diet adopts a metabolic state that favors pyruvate/acetyl-CoA production and macromolecule biosynthesis

Oogenesis is a resource-intensive process (Spradling 1993); we therefore reasoned that the status of energy metabolism in adipocytes might influence ovarian processes. Glycolysis is a major metabolic pathway that converts glucose into pyruvate through multiple intermediate metabolites. Under aerobic conditions, pyruvate is typically transported into the mitochondria and converted into acetyl-CoA, which fuels the citric acid cycle. NADH and $FADH_2$, high-energy compounds generated during the citric acid cycle, are then transferred to the electron transport chain to drive high levels of ATP synthesis through oxidative phosphorylation (Figure S2 in File S1). Under anabolic conditions, however, glycolytic intermediates can instead fuel biosynthetic pathways to produce biomolecules, including nucleotides from glucose-6P, amino acids from 3-phosphoglycerate, or lipids from pyruvate (through acetyl-CoA) (Figure S2 in File S1). Thus, we first examined glycolysis, citric acid cycle and oxidative phosphorylation enzymes.

There is a marked shift in adipocyte glucose metabolism enzymes between rich and poor diets. Hex-C, which irreversibly converts glucose to glucose-6-phosphate and is one of the regulatory enzymes in glycolysis (Moser *et al.* 1980), was more abundant on a rich diet (Figure 1E and Figure 4A and Table S4). By contrast, a number of regulatory enzymes involved in the citric acid cycle and oxidative phosphorylation, including Citrate synthase (Kdn) (Fergestad *et al.* 2006), ATP synthase-β (ATPsyn-β), Sluggish-A (SlgA) (Hayward *et al.* 1993) and Glutamic oxaloacetate aminotransferase-2 (Got2) (Grell 1976), had lower levels on a rich diet (Figure 4A and Table S4), suggesting that the increased levels of Hex-C (and of metabolized glucose) fuel the production of building blocks in addition to ATP generation. In accordance, two regulatory enzymes that catalyze the production of cytosolic acetyl-CoA (a fatty acid precursor) had elevated levels on a rich diet: acetyl-CoA synthase (AcCoAS) produces cytosolic acetyl-CoA from acetate while ATP citrate lyase (ATPCL) produces cytosolic acetyl-CoA from citrate transported from mitochondria to the cytosol (Seegmiller *et al.* 2002) (Figure 4A and Table S4). Fatty acid synthase 1 (FASN1), an enzyme involved in fatty acid production from cytosolic acetyl-CoA (Garrido *et al.* 2015), was more highly expressed on a rich diet, as were enzymes involved in nucleic acid and amino acid metabolism (Figure S2 in File S1). Pepck, an enzyme that catalyzes a regulatory step of gluconeogenesis (Montal *et al.* 2015), was also upregulated on a rich diet (Figure 4A and Figure S4 in File S1); the product of this reaction, phosphoenolpyruvate, can also be converted into pyruvate and cytosolic acetyl-CoA (Montal *et al.* 2015) (Figure 4A). Adipocyte mitochondrial mass and membrane potential did not appear to increase despite the higher nutritional input from a rich diet (Figure 4, B–D), lending further support to the idea of preferential building block production. The fat body, however, is composed of postmitotic cells (Johnson and Butterworth 1985) that are not growing when females are maintained continuously on a rich diet (Figure S1D in File S1), suggesting that this anabolic state of the fat body may instead non cell-autonomously support other rapidly growing tissues, such as the ovary.

Enzymes regulating glucose consumption and cytosolic acetyl-CoA production in adipocytes promote early germline cyst survival

We next asked if diet-regulated enzymes involved in glycolysis and pyruvate/acetyl-CoA production in adipocytes influence oogenesis, focusing on Hex-C, Pepck, ATPCL, and AcCoAS, which are more abundant on a rich diet (Figure 1E, Figure 4A, Figure 5A and Table S4). To knockdown these enzymes specifically in adult adipocytes, we used the previously described *tubGal80^{ts}*; *3.1Lsp2-gal4* (*Lsp2^{ts}*) system (Armstrong *et al.* 2014) to drive *UAS* RNAi lines (see Figure 5B). Adult adipocyte-specific knockdown of *Hex-C*, *Pepck*, *ATPCL*, and *AcCoAS* did not lead to consistent changes in GSC maintenance, GSC proliferation, or vitellogenesis (Figure S3, A–C in File S1), or in stored lipid levels in adipocytes (Figure 5, G–M) relative to *luciferase* (*luc*) RNAi control. By contrast, we detected a significant increase in cell death of early germline cysts in the germaria of females at 7 and 14 days of *Hex-C* or *Pepck* adipocyte RNAi knockdown (Figure 5C; see Figure S3D in File S1 for *UAS*-only controls). In fact, because of the increase in early germline cyst death at 7 and 14 days in *Hex-C* and *Pepck* adipocyte RNAi females (Figure 5C), those germaria were considerably smaller than control germaria (Figure 5, D–F). We did not observe this early cyst death phenotype in *ATPCL* and *AcCoAS* adipocyte RNAi females (Figure 5C), likely due to mutual compensation of these enzymes, as described in mammals (Wellen *et al.* 2009; Zhao *et al.* 2016). These results suggest that enzymes involved in glycolysis and biosynthesis in adipocytes non cell-autonomously ensure optimal survival of early GSC progeny at a diet-sensitive oogenesis checkpoint (Drummond-Barbosa and Spradling 2001). Nevertheless, it remains unclear whether the regulation of these enzymes by diet *per se* is physiologically relevant to early germ cells.

Adipocyte β oxidation enzymes support GSC maintenance

Multiple enzymes involved in β oxidation of fatty acids had higher levels on a rich diet, suggesting that dietary fatty acids might serve as a significant source of mitochondrial acetyl-CoA for generation of ATP through oxidative phosphorylation in the fat body (Figure 6A and Table S4). Among regulatory enzymes enriched on a rich diet are two acyl-CoA oxidases [CG5009 and acyl-CoA oxidase at 57D proximal (Acox57D-p)] predicted to reside in the peroxisome (Faust *et al.* 2012; Baron *et al.* 2016), and long-chain acyl-CoA synthase (CG3961) and short-chain acyl-CoA dehydrogenase (Arc42), which are

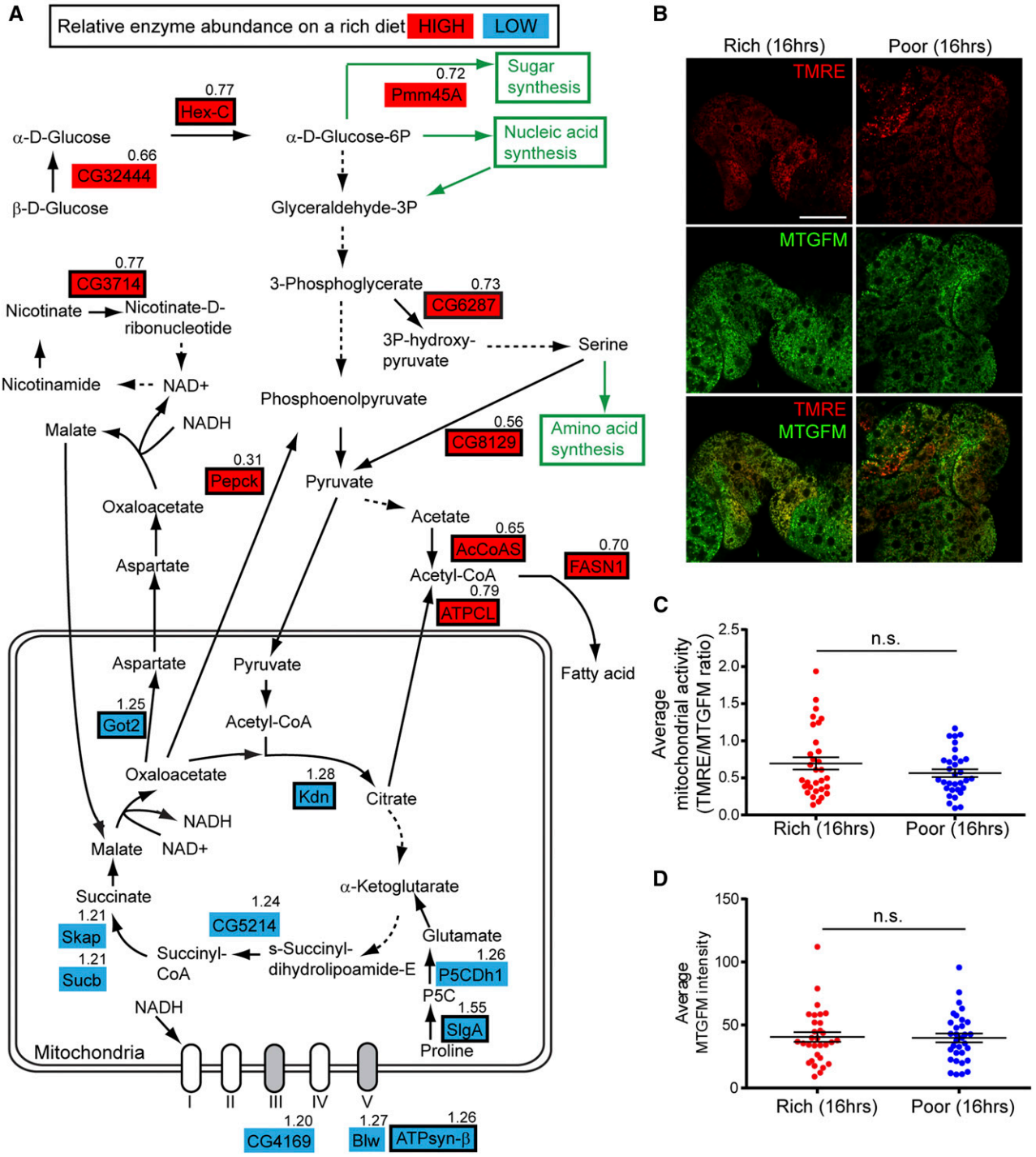

Figure 4 The metabolism of the fat body on a rich diet favors pyruvate/acetyl-CoA production and macromolecule biosynthesis. (A) Diagram of diet-dependent changes in the levels of metabolic enzymes in the glycolytic pathway, citric acid cycle, and electron transport chain. Enzymes showing relatively high or low abundance on a rich diet are highlighted in red or blue, respectively. Regulatory enzymes are indicated by a black rectangular outline. Poor to Rich iTRAQ (isobaric tags for relative and absolute quantification) ratio is shown for each metabolic enzyme. Solid arrows indicate direct conversion of metabolites, whereas dashed arrows signify multiple enzymatic steps. Regulatory enzymes that contribute to pyruvate/acetyl-CoA production, including Hex-C (Hexokinase-C), Pepck (phosphoenolpyruvate carboxykinase), AcCoAS (acetyl-CoA synthase), and ATPCL (ATP citrate lyase) are upregulated on a rich diet, whereas regulatory enzymes in the citric acid cycle and electron transport chain are downregulated on a rich diet, suggesting that the fat body favors building block production. (B) Live adipocytes from females maintained for 16 hr either on rich or poor diet simultaneously stained with the membrane potential-dependent mitochondrial dye tetramethylrhodamine, ethyl ester (TMRE) and the membrane potential-independent mitochondrial dye Mitotracker Green FM (MTGFM). Scale bar, 40 μm. (C and D) Average normalized mitochondrial activity (TMRE/MTGFM ratio) (C) and average MTGFM intensity (proportional to total mitochondrial mass) (D) in adipocytes from females illustrated in (B) (n = 31 adipocyte fields for Rich and n = 32 adipocyte fields for Poor; 16 females were examined for each dietary condition). n.s., not significant, Student's t-test.

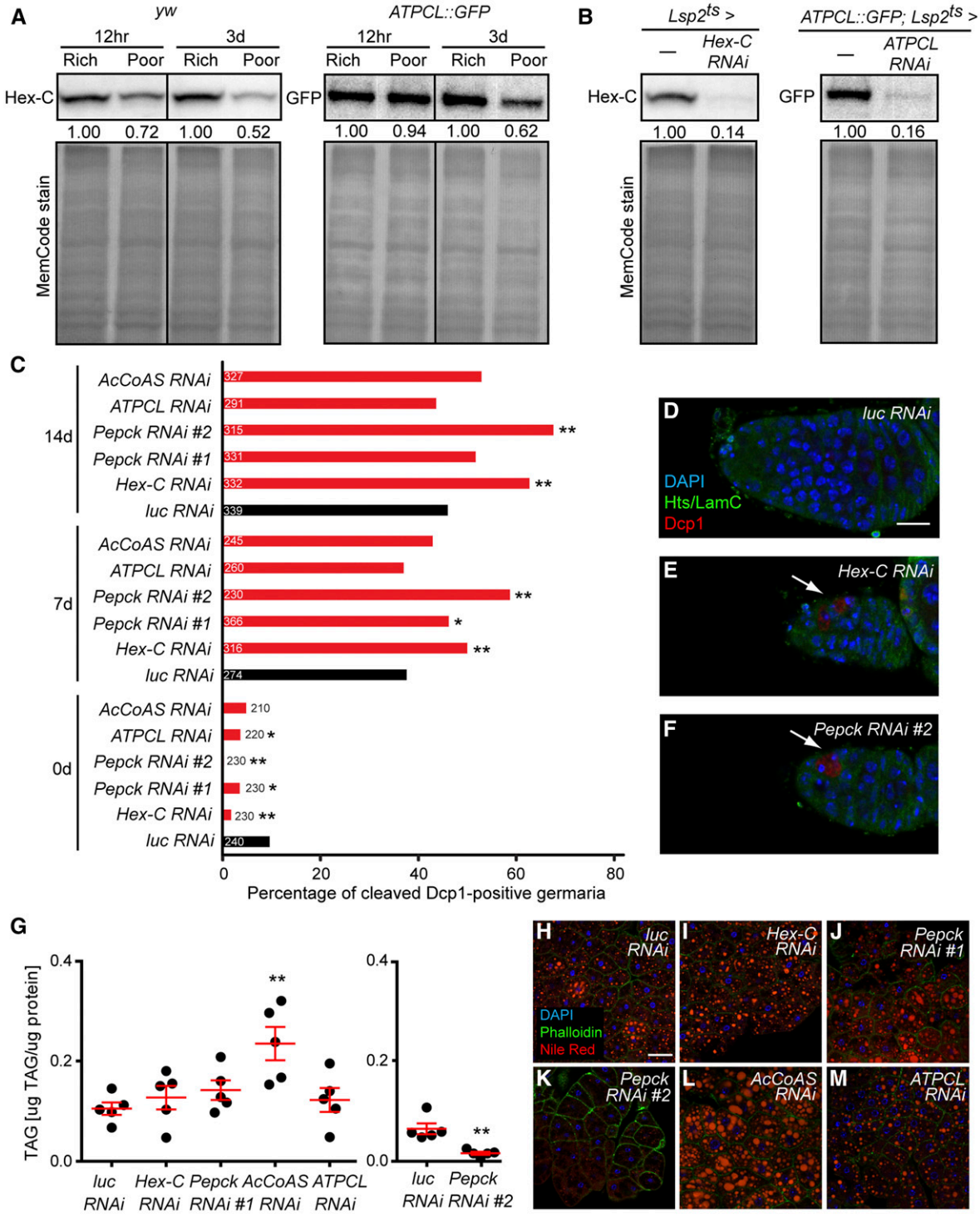

Figure 5 Regulatory enzymes involved in pyruvate/acetyl-CoA production in adipocytes promote survival of early germline cysts. (A) Western blots showing expression of Hex-C and ATPCL::GFP in dissected fat bodies at 12 hr and 3 days on rich *vs.* poor diets. The expression levels on a poor diet were normalized to those on a rich diet for each time point. Total loaded proteins are shown with MemCode stain. (B) Western blotting analysis of Hex-C and ATPCL::GFP in fat body at 7 days of *Lsp2*^{ts}-mediated RNAi against *Hex-C* and *ATPCL*, respectively. Total proteins are used as a loading control (bottom). (C) Percentage of germaria containing cleaved Dcp1-positive cysts at 0, 7, or 14 days of *Lsp2*^{ts}-mediated RNAi against *Hex-C*, *Pepck*, *ATPCL* and *AcCoAS*. The number of germaria analyzed from three independent experiments is shown inside or to the right of bars. $*P < 0.05$, $**P < 0.01$, Chi-square test. (D–F) Germaria of females subjected to 14 days of *Lsp2*^{ts}-mediated *luciferase* (*luc*) control (D), *Hex-C* (E), or *Pepck* (F) RNAi knockdown. Hts (green), fusome; Lamin C (green), cap cell nuclear envelope; cleaved Dcp1 (red), dying cystoblasts/cysts; DAPI (blue), nuclei. Arrows indicate dying germ cells. Scale bar, 10 μm. (G) TAG contents (μg TAG/μg protein) in dissected fat bodies at 7 days of *Lsp2*^{ts}-mediated RNAi against *luc* control, *Hex-C*, *Pepck*, *AcCoAS* and *ATPCL*. $**P < 0.01$, Student's *t*-test. (H–M)

involved in mitochondrial β oxidation. This is consistent with the fact that the poor diet lacks lipids, whereas the rich diet contains dietary lipids that can be used as energy source.

To examine if fatty acid oxidation in adipocytes affects the GSC lineage, we knocked down long-chain acyl-CoA synthase/CG3961 in adult adipocytes using two independent RNAi lines. When *CG3961* was knocked down, adipocyte TAG levels significantly increased (Figure 6, B–D), suggesting that fatty acids are not properly broken down. Similarly, adipocyte-specific knockdown of the CG3961 mammalian homolog ACSL1 (Faust *et al.* 2012; Baron *et al.* 2016) also leads to impaired fatty acid oxidation and increased TAG content in mice (Ellis *et al.* 2010). Although *CG3961* knockdown in adult adipocytes did not affect GSC proliferation, early germline cyst survival, or vitellogenesis (Figure S4, A–C in File S1), it led to a significant increase in the rate of GSC loss (Figure 6, E–G, see Figure S4G in File S1 for *UAS*-only controls). It is possible that ATP produced from fatty acid oxidation supports processes (*e.g.*, secretion or production of specific molecules) within adipocytes that are important for maintenance of GSCs. Alternatively, fatty acid oxidation could affect the ovary through the production of ketone bodies, which can be exported to other organs as a source of energy (Bartlett and Eaton 2004) or for signaling purposes (Newman and Verdin 2014).

PE synthesis enzymes in adipocytes contribute to GSC maintenance

Several enzymes that generate a major membrane-bound glycerophospholipid in *Drosophila*, PE (Jones *et al.* 1992), are regulated by diet (Figure 6A and Table S4). Sphingosine-1-phosphate lyase (Sply) (Herr *et al.* 2003) and Ethanolamine kinase (Eas) (Pavlidis *et al.* 1994), regulatory enzymes involved in PE generation, as well as Phosphatidylserine synthase 1 (CG4825), a regulatory enzyme that produces phosphatidylserine [which can be converted to PE (Vance and Tasseva 2013)], were more highly expressed on a rich diet. The higher levels of Eas and CG4825 on a rich diet were confirmed by Western blotting (Figure 6H). These observations are interesting because PE has diverse roles in membrane structure, metabolic regulation, membrane fusion, post-translational modifications, autophagy, and the production of signaling lipids (Vance and Tasseva 2013; Wellner *et al.* 2013).

To address if PE synthesis in adipocytes influences oogenesis, we performed *Lsp2^{ts}*-mediated adult adipocyte-specific RNAi of *eas* and *CG4825*. The knockdown was effective, based on the marked reduction in protein levels (Figure 6I). In agreement with the reported function of PE in repressing lipogenesis through SREBP inhibition in *Drosophila* (Dobrosotskaya *et al.* 2002; Seegmiller *et al.* 2002), *eas* and *CG4825* knockdown led to increased TAG levels (Figure 6, B and J–L). Upon adult adipocyte-specific knockdown of *eas* and *CG4825*, GSCs were lost at significantly higher rates compared to controls, suggesting that PE synthesis in adipocytes contributes to normal GSC maintenance (Figure 6, M–O; see Figure S4G in File S1 for *UAS*-only controls). GSC proliferation, early germline cyst survival, and vitellogenesis were unaffected in *eas* and *CG4825* knockdown females (Figure S4, D–F in File S1), indicating that PE synthesis in adipocytes specifically affects GSC maintenance.

Lipid transport from adipocytes is required for follicle progression through vitellogenesis

In addition to being locally consumed, lipids can also be transported from adipocytes to influence peripheral tissues (Canavoso *et al.* 2001). The apolipoprotein B-family lipoprotein Lipophorin (Lpp), the major hemolymph lipid carrier in *Drosophila* (Palm *et al.* 2012), showed slightly reduced levels on a poor diet based on our iTRAQ analysis, although this reduction did not reach the iTRAQ cut-off (Table S1). We found that adult adipocyte-specific knockdown of *Lpp* (Figure 7A) results in a ~90% block in vitellogenesis due to follicle degeneration (Figure 7, B and C). This phenotype is indistinguishable from that resulting from loss of the Lpp receptor required in the ovary (Parra-Peralbo and Culi 2011), indicating that Lpp transports lipids directly from adipocytes to the ovary. We also observed an increase in GSC loss upon adipocyte knockdown of *Lpp* (Figure S5A in File S1), possibly owing to reduced levels of ecdysone, a steroid hormone known to be produced by later vitellogenic follicles (Schwartz *et al.* 1985; Huang *et al.* 2008) and required for GSC maintenance (Ables and Drummond-Barbosa 2010). Not surprisingly, egg production in adipocyte-specific *Lpp* RNAi females is reduced (Figure S5B in File S1). There are no consistent defects in early germline cyst survival in *Lsp2^{ts}*-mediated *Lpp* RNAi females (Figure S5C in File S1), underscoring the specificity of ovarian phenotypes resulting from adipocyte manipulation.

Systemic iron homeostasis contributes to GSC maintenance

Several other nutrients are transported by the circulatory system with the help of carrier proteins (Linder *et al.* 1998; Alpers 2016), prompting us to search our iTRAQ data for secreted metabolic proteins. Among 50 putative secreted proteins regulated by diet, several are involved in metabolic processes, including purine metabolism, iron homeostasis, and insulin regulation (Table S5). One of those proteins is Ferritin 1 Heavy Chain Homolog (Fer1HCH), the heavy subunit of Ferritin 1, which stores intracellular iron but can also be secreted into the hemolymph for iron transport (Nichol and Locke 1990; Tang and Zhou. 2013a,b). Following a slight

Adipocytes at 7 days of *Lsp2^{ts}*-mediated RNAi against *luc* control, *Hex-C*, *Pepck*, *AcCoAS* and *ATPCL*. DAPI (blue), nuclei; Phalloidin (green), actin; Nile Red (red), lipid droplets. Scale bar, 40 μm. AcCoAS, acetyl-CoA synthase; ATPCL, ATP citrate lyase; Hex-C, hexokinase-C; *luc*, *luciferase*; Pepck, phosphoenolpyruvate carboxykinase; RNAi, RNA interference; TAG, triacylglycerol.

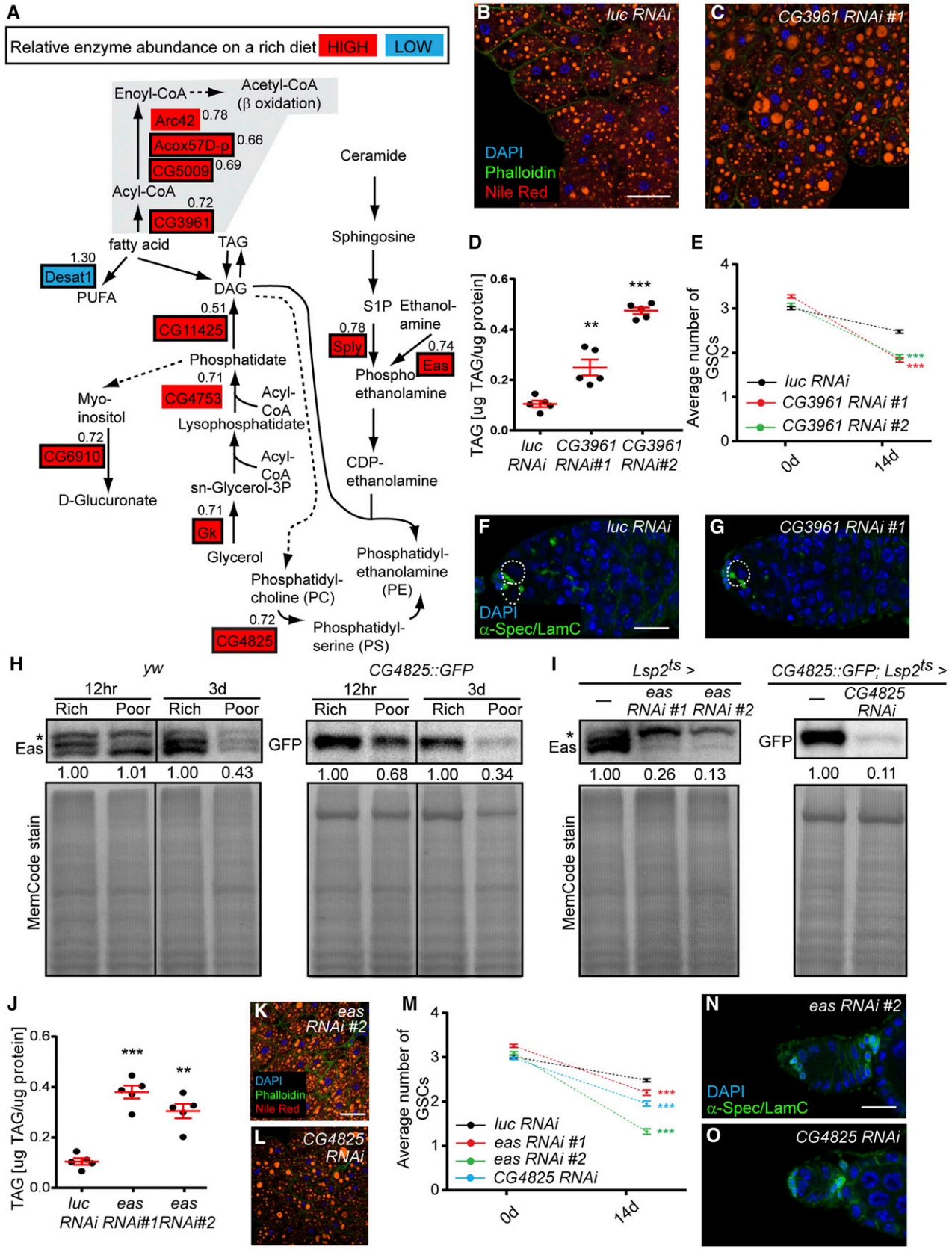

Figure 6 Regulatory enzymes involved in fatty acid oxidation and PE synthesis in adipocytes promote GSC maintenance. (A) Diagram of diet-dependent changes in the levels of metabolic enzymes regulating fatty acid utilization. Metabolic enzymes showing relatively high or low abundance on a rich diet are highlighted in red or blue, respectively. Regulatory enzymes are indicated by a black rectangular outline. Poor to Rich iTRAQ ratio is shown for each

increase in Fer1HCH levels in the fat body at 12 hr, its levels become reduced by 3 days on a poor diet, likely as a result of its secretion into the hemolymph (Figure 1E and Figure 7D). Adult adipocyte-specific knockdown of *Fer1HCH* (Figure 7E) did not affect GSC proliferation, early germline cyst survival, or vitellogenesis (Figure S6, A–C in File S1); however, GSC maintenance was significantly impaired (Figure 7, F–H; see Figure S6D in File S1 for *UAS*-only controls). The absence of gross morphological defects in adipocytes other than a slight reduction in cell size upon *Fer1HCH* knockdown (Figure 7, I and J) and the fact that multiple oogenesis processes are unaffected rule out the possibility that the GSC loss phenotype is caused by global adipocyte dysfunction. These data suggest that iron transport from adipocytes and/or iron detoxification in adipocytes are required for proper maintenance of GSCs. Given that hemolymph levels of Fer1HCH increase on a poor diet (Figure 7D), we speculate that Fer1HCH might prevent excessive GSC loss under nutrient limitation.

Discussion

Adipocytes have key physiological roles, and their dysfunction promotes a number of diseases, including cancers. Our recent work showed that amino acid sensing by adipocytes is transmitted to the *Drosophila* GSC lineage to modulate GSC numbers and ovulation (Armstrong *et al.* 2014). Here, we took an unbiased proteomic approach to identify early changes in metabolic protein levels in adipocytes in response to diet, combined with functional testing of key regulatory enzymes for roles in the ovary. We identified a number of metabolic pathways that respond rapidly to dietary changes, reflecting a shift of glucose metabolism toward pyruvate/acetyl-CoA production and biosynthetic processes, and increased fatty acid oxidation and PE synthesis on a rich diet. Adipocyte-specific knockdown of regulatory enzymes suggests specific roles for pyruvate/acetyl-CoA production in early germline cyst survival, and for fatty acid oxidation and PE synthesis in GSC maintenance. Nutrient carrier protein levels are also regulated by diet, and lipid and iron transport from adipocytes modulate vitellogenesis and GSC number, respectively (Figure 7K). Our studies, however, did not directly address whether the actual regulation of the levels of these metabolic proteins by diet indeed contributes to how the ovary responds to dietary changes. Nevertheless, these results open the door to future investigation of the mechanisms whereby metabolic pathways in adipocytes modulate tissue stem cells and their differentiating progeny, and of how disruption or cooption of such processes in obese individuals might contribute to pathological conditions.

Pyruvate/acetyl-CoA production and biosynthesis in adipocytes and germline cyst survival

Our finding that Pepck or Hex-C knockdown in adipocytes leads to a significant increase in germline cyst death suggests that pyruvate/acetyl-CoA production, biosynthetic processes, or both promote survival of early GSC progeny. It is conceivable that early germline cysts might sense the abundance of biomolecules, including fatty acids [perhaps through G protein-coupled receptors (Blad *et al.* 2012)], produced by adipocytes such that oogenesis can proceed past this early checkpoint when dietary conditions are favorable. This "selfless" scenario of one organ altering its metabolism to support a distinct organ is in contrast to the Warburg effect observed in cancers and other rapidly growing cells, in which aerobic glycolysis and biosynthesis cell-autonomously benefit growth (Vander Heiden *et al.* 2009; Tennessen *et al.* 2011). Recent studies, however, suggest that cancer growth can also be supported by altered metabolic states of otherwise normal nearby cells (Nieman *et al.* 2011; Whitaker-Menezes *et al.* 2011). Cancer growth can also be supported by altered metabolism of more distant tissues, as in the case of cachexia, which results from systemic effects of cancer cells

metabolic enzyme. Solid arrows indicate a direct reaction, whereas dashed arrows signify multiple enzymatic reactions. (B and C) Adipocytes at 7 days of *Lsp2^{ts}*-mediated RNAi against *luc* control and *CG3961*. DAPI (blue), nuclei; Phalloidin (green), actin; Nile Red (red), lipid droplets. Scale bar, 40 μm. (D) TAG contents (μg TAG/μg protein) in fat body at 7 days of *Lsp2^{ts}*-mediated RNAi against *luc* control and *CG3961*. $^{**}P < 0.01$, $^{***}P < 0.001$, Student's *t*-test. (E) Average number of GSCs per germarium at 0 and 14 days of *Lsp2^{ts}*-mediated RNAi against *luc* control and *CG3961*. Numbers of germaria analyzed from three independent experiments are: 245 for *luc* control RNAi 0d; 270 for *luc* control RNAi 14d; 225 for *CG3961* RNAi #1 0d; 270 for *CG3961* RNAi #1 14d; 253 for *CG3961* RNAi #2 0d; and 270 for *CG3961* RNAi #2 14d. $^{***}P < 0.001$, two-way ANOVA with interaction. (F and G) Examples of germaria at 14 days of *Lsp2^{ts}*-mediated RNAi against *luc* control and *CG3961*. α-Spectrin (green), fusome; Lamin C (green), cap cell nuclear envelope; DAPI (blue), nuclei. GSCs are outlined. Scale bar, 10 μm. (H) Western blots of Eas and CG4825::GFP in fat bodies at 12 hr or 3 days on rich *vs.* poor diets. The expression levels on a poor diet are normalized to those on a rich diet for each time point. Total loaded protein shown with MemCode stain below. (I) Western blots of Eas and CG4825::GFP in fat body at 7 days of *Lsp2^{ts}*-mediated RNAi against *eas* and *CG4825*. Total protein shown as a loading control (bottom). Asterisks in (H) and (I) indicate nonspecific bands (Pascual *et al.* 2005). (J) TAG contents (μg TAG/μg protein) in fat body at 7 days of *Lsp2^{ts}*-mediated RNAi against *luc* control and *eas*. $^{**}P < 0.01$, $^{***}P < 0.001$, Student's *t*-test. Experiments in (D) and (J) were conducted in parallel, and same control data (*luc* RNAi) are shown in both graphs. (K and L) Adipocytes stained as in (B and C) at 7 days of *Lsp2^{ts}*-mediated RNAi against *eas* and *CG4825*. Scale bar, 40 μm. (M) Average number of GSCs per germarium at 0 and 14 days of *Lsp2^{ts}*-mediated RNAi against *luc* control, *eas*, and *CG4825*. Numbers of germaria analyzed from three independent experiments are: 245 for *luc* control RNAi 0d; 270 for *luc* control RNAi 14d; 256 for *eas* RNAi #1 0d; 260 for *eas* RNAi #1 14d; 258 for *eas* RNAi #2 0d; 252 for *eas* RNAi #2 14d; 250 for *CG4825* RNAi 0d; 260 for *CG4825* RNAi 14d. $^{***}P < 0.001$, two-way ANOVA with interaction. Experiments in (E) and (M) were conducted in parallel, and the same control data (*luc* RNAi) are shown in both graphs. (N and O) Examples of germaria at 14 days of *Lsp2^{ts}*-mediated RNAi against *eas* and *CG4825*, labeled with α-Spectrin (green, fusome), Lamin C (green, cap cell nuclear envelope), and DAPI (blue, DNA). No GSCs are present in these germaria of *eas* and *CG4825* adipocyte RNAi females (compare to F). Scale bar, 10 μm. CG4825, phosphatidylserine synthase 1; Eas, easily shocked; GSC, germline stem cell; iTRAQ, isobaric tags for relative and absolute quantification; *luc*, *luciferase*; PE, phosphatidylethanolamine; RNAi, RNA interference; TAG, triacylglycerol.

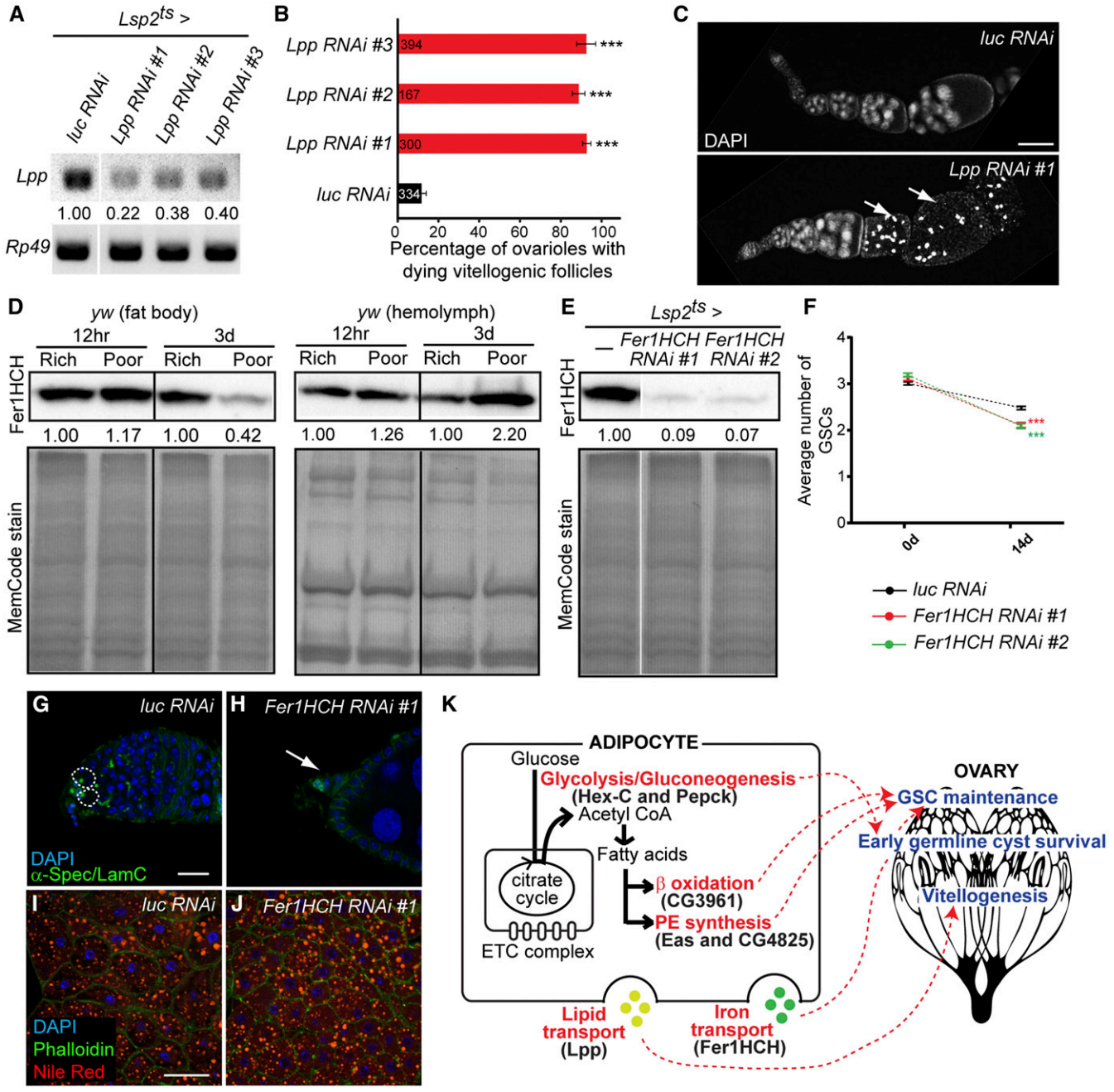

Figure 7 Lipid and iron transport from adipocytes affects vitellogenesis and germline stem cell (GSC) maintenance, respectively. (A) RT-PCR analysis of *Lipophorin* (*Lpp*) mRNA expression in the fat body at 7 days of *Lsp2*^{ts}-mediated RNA interference (RNAi) induction against *Lpp* showing knockdown of *Lpp*. Relative *Lpp* expression levels in *Lpp* RNAi normalized to that in *luc* RNAi control are shown. *Rp49* is used as a control. (B) Percentage of ovarioles with dying vitellogenic follicles based on pyknotic nuclei at 7 days of *Lsp2*^{ts}-mediated RNAi against *luc* control and *Lpp* using three different RNAi lines. The number of ovarioles analyzed from three independent experiments is shown inside bars. ***$P < 0.001$, Student's *t*-test. Data shown as mean ± SEM (C) Ovarioles stained with DAPI (nuclei) at 7 days of *Lsp2*^{ts}-mediated RNAi against *luc* control and *Lpp*. Arrows indicate dying vitellogenic follicles. (D) Western blots of Ferritin 1 Heavy Chain Homolog (Fer1HCH) in dissected fat bodies and extracted hemolymph at 12 hr or 3 days on rich or poor diets. Fer1HCH levels decrease in the fat body and increase in the hemolymph over time on a poor diet, indicating increased secretion. Fer1HCH levels on a poor diet are normalized to those on a rich diet for each time point. Total loaded proteins are shown with MemCode stain below. (E) Western blotting analysis of Fer1HCH expression levels in fat body at 7 days of *Lsp2*^{ts}-mediated RNAi against *Fer1HCH*. Total proteins are used as a loading control (bottom). (F) Average number of GSCs per germarium at 0 and 14 days of *Lsp2*^{ts}-mediated RNAi against *luc* control and *Fer1HCH*. Numbers of germaria analyzed from three independent experiments are: 245 for *luc* control RNAi 0d; 270 for *luc* control RNAi 14d; 227 for *Fer1HCH* RNAi #1 0d; 260 for *Fer1HCH* RNAi #1 14d; 223 for *Fer1HCH* RNAi #2 0d; and 260 for *Fer1HCH* RNAi #2 14d. ***$P < 0.001$, two-way ANOVA with interaction. These experiments were done in parallel to those in Figure 6, E and M and the same control data (*luc* RNAi) are plotted. (G and H) Germaria at 14 days of *Lsp2*^{ts}-mediated RNAi against *luc* control or *Fer1HCH*, showing a severe example of GSC loss in (H), with the very small germarium indicated by an arrow. α-Spectrin (green), fusome; Lamin C (green), cap cell nuclear envelope; DAPI (blue), nuclei. GSCs are

on the metabolism of adipose tissue and muscle (Martinez-Outschoorn *et al.* 2014). These are interesting parallels between the physiological coupling of *Drosophila* adipocytes and ovarian tissues, and the pathological setting of cancers forcing normal cells to fuel cancerous growth.

In addition to its roles in fatty acid biosynthesis and other metabolic processes, acetyl-CoA is emerging as a major regulator of acetylation of histones and other proteins (Pietrocola *et al.* 2015). Reversible protein acetylation integrates metabolic status and multiple processes within cells (Menzies *et al.* 2016), while histone acetylation in particular is associated with active gene expression, linking cell metabolism to the epigenetic state of cells (Janke *et al.* 2015). In this context, it is interesting that adipocyte nuclei become more compact on a poor diet relative to a rich diet over time (Figure S1,E in File S1). Future studies should investigate the role of acetyl-CoA level regulation on the epigenetic state and transcriptome of adipocytes on different diets, and their potential relationship to the control of early germline cyst survival.

Fatty acid oxidation in adipocytes and GSC maintenance: energy or metabolic signals?

Our iTRAQ data suggest that not only is acetyl-CoA produced from pyruvate converted to fatty acids, but that fatty acids are also used as a source of energy through β oxidation. While these observations may appear contradictory, one potential interpretation is that adipocytes have a very high demand for fatty acids both for their own consumption as a source of energy and for export to growing oocytes. Adipocytes may upregulate β oxidation when dietary lipids are available, and also convert sugars into additional fatty acids to ensure optimal supply for ovarian export.

The adipocyte-specific requirement for CG3961, the homolog of mammalian ACSL1 (Ellis *et al.* 2010), for the proper maintenance of GSCs suggests that production of either ATP or ketone bodies plays an important role in this process. ATP is used for a wide range of physiological processes, and it is possible that the production and/or secretion of key adipocyte factors are impaired in low ATP conditions. However, β oxidation can also support the production of ketone bodies at the expense of the oxidative phosphorylation of acetyl-CoA (Bartlett and Eaton 2004). Ketone bodies, in turn, can be exported as an alternative source of energy to other tissues, or they may act as signaling metabolites (Newman and Verdin 2014).

Possible mechanisms for the connection between PE synthesis in adipocytes and GSCs

Our data suggest that adipocyte PE synthesis controls GSC numbers. An abundant membrane phospholipid, PE also has a number of regulatory roles. PE can modulate G protein-coupled receptor signaling (Dijkman and Watts 2015; Dawaliby *et al.* 2016) and it can also be a donor of ethanolamine for the covalent modification of proteins, including the eukaryotic elongation factor eEF1A and the autophagy protein LC3 (Vance *et al.* 2013). In *Drosophila*, analogous to cholesterol in mammals (Brown and Goldstein 1997), PE regulates the transcriptional factor SREBP, which controls lipogenic enzyme expression (Dobrosotskaya *et al.* 2002; Seegmiller *et al.* 2002). PE production in adipocytes could also potentially be converted to more direct signals to the germline. For example, PE has been shown to serve as a ligand for mammalian nuclear receptors SF-1 and LRH-1, with different effects depending on fatty acyl groups in the sn-1 and sn-2 positions (Forman 2005). Both SF-1 and LRH-1 have known roles in the development and function of reproductive organs (Yazawa *et al.* 2015), and their *Drosophila* homolog, Hr39 (Ohno and Petkovich 1993), is required for proper formation and function of the female reproductive system (Allen and Spradling 2008; Sun and Spradling 2012). However, Hr39 is not required for GSC maintenance based on the analysis of strong hypomorphic alleles (Ables *et al.* 2016), likely ruling out its role in a PE-dependent mechanism for GSC control. Finally, PE (combined with phosphatidylcholine) can serve as a source of precursors for the synthesis of the endocannabinoid anandamide (Wellner *et al.* 2013).

Transported nutrients as regulators of stem cell lineages?

In addition to metabolic enzymes, we also found that nutrient carriers have specific roles in the GSC lineage, with Fer1HCH being required for maintenance of the proper number of GSCs, and Lpp controlling vitellogenesis. The major function of mammalian Ferritin is to store iron intracellularly, with iron transport primarily accomplished by the Transferrin–Transferrin receptor system (Tang and Zhou 2013b). However, a fraction of Ferritin exists in circulation and has recently been shown to deliver iron to other cells (Todorich *et al.* 2008; Li *et al.* 2009; Wang *et al.* 2010). The specific phenotypes that we observe from disruption of nutrient transport from adipocytes suggest that interorgan nutrient transport may impact tissue stem cell lineages more generally.

Prospects

This study opens a wealth of future areas of investigation. It will be interesting to investigate the nature of the signals downstream of various metabolic pathways with specific roles in the germline. Such signals may include nutrients, metabolites, proteins, or any other types of molecules with signaling

outlined. Scale bar, 10 μm. (I and J) Adipocytes at 7 days of *Lsp2*^{ts}-mediated RNAi against *luc* control and *Fer1HCH*. DAPI (blue), nuclei; Phalloidin (green), actin; Nile Red (red), lipid droplets. Scale bar, 40 μm. (K) Model for germline control by adipocyte metabolism. Hex-C (Hexokinase-C) and Pepck (Phosphoenolpyruvate carboxykinase) ensure the survival of early germline cysts, whereas Eas (Ethanolamine kinase), CG4825 (Phosphatidylserine synthase 1), and CG3961 (Long-chain acyl-CoA synthase) help maintain GSCs, suggesting that adipocyte metabolic pathways refine the regulation of diet-dependent steps of oogenesis. Adipocyte lipid transport by Lipophorin (Lpp) and iron transport by Fer1HCH also contribute to the control of vitellogenesis and GSC maintenance, respectively. Thick black arrows indicate relatively high abundance of metabolic enzymes in these pathways on a rich diet compared to a poor diet. ETC, electron transport chain.

roles. They may signal through a variety of receptors directly to germ cells in the ovary or indirectly, through nearby somatic cells or even intermediate organs via relay endocrine signals. Future studies will also be required to determine to what extent diet-induced changes in the levels of adipocyte regulatory metabolic enzymes and nutrient transporters is physiologically relevant to how the ovary responds to dietary changes, and how diet controls metabolic protein levels in adipocytes. Dietary nutrients may be directly sensed by adipocytes or they may be sensed through other organs, which then communicate to adipocytes via intermediate molecules. Finally, it will be important to expand these studies on the link between adipocyte metabolism and stem cell regulation to a wide range of stem cell systems in various organisms.

Acknowledgments

We thank R. Cole for overseeing the isobaric tags for relative and absolute quantification (iTRAQ) analysis conducted by the Mass Spectrometry and Proteomics Facility, Johns Hopkins University School of Medicine, and C. Talbot for assistance with iTRAQ statistical analysis. We thank A. Spradling, T. Preat, J. Kim-Ha, B. Zhou, P. Jordan, the Bloomington *Drosophila* Stock Center [supported by the National Institutes of Health (NIH): P40 OD 018537], the Kyoto *Drosophila* Genomics and Genetic Resources, the Vienna *Drosophila* RNAi Stock Center, the Transgenic RNAi Project at Harvard Medical School, and the Developmental Studies Hybridoma Bank for fly stocks and reagents. We also thank F. Wan for use of Western blot chemiluminescent imager, and M. Sieber for helpful scientific discussions. Finally, we thank M. Sieber, L. Weaver, and T. Ma for valuable comments on this manuscript. This work was supported by NIH grant R01 GM 069875 (D.D.-B.). A.R.A. was supported by NIH grant F32 GM 106718, and K.M.L. was supported by NIH grant T32 CA 009110. The authors declare no competing financial interests.

Author contributions: S.M. performed all experiments in this manuscript, with the following exceptions: A.R.A. performed Lpp experiments described in Figure 7, A–C and Figure S5 in File S1; L.L.S. and K.M.L. performed all dissections and protein sample preparations before submitting them to the Mass Spectrometry and Proteomics Facility for iTRAQ analysis. S.M., A.R.A., and D.D.-B. designed and analyzed experiments. S.M. and D.D.-B. wrote the manuscript, with final editorial input from all authors.

Literature Cited

Ables, E. T., and D. Drummond-Barbosa, 2010 The steroid hormone ecdysone functions with intrinsic chromatin remodeling factors to control female germline stem cells in Drosophila. Cell Stem Cell 7: 581–592.

Ables, E. T., K. M. Laws, and D. Drummond-Barbosa, 2012 Control of adult stem cells in vivo by a dynamic physiological environment: diet-dependent systemic factors in Drosophila and beyond. Wiley Interdiscip. Rev. Dev. Biol. 1: 657–674.

Ables, E. T., G. H. Hwang, D. S. Finger, T. D. Hinnant, and D. Drummond-Barbosa, 2016 A genetic mosaic screen reveals Ecdysone-responsive genes regulating Drosophila Oogenesis. G3 6: 2629–2642.

Allen, A. K., and A. C. Spradling, 2008 The Sf1-related nuclear hormone receptor Hr39 regulates Drosophila female reproductive tract development and function. Development 135: 311–321.

Alpers, D. H., 2016 Absorption and blood/cellular transport of folate and cobalamin: pharmacokinetic and physiological considerations. Biochimie 126: 52–56.

Armstrong, A. R., K. M. Laws, and D. Drummond-Barbosa, 2014 Adipocyte amino acid sensing controls adult germline stem cell number via the amino acid response pathway and independently of target of rapamycin signaling in Drosophila. Development 141: 4479–4488.

Arrese, E. L., and J. L. Soulages, 2010 Insect fat body: energy, metabolism, and regulation. Annu. Rev. Entomol. 55: 207–225.

Baron, M. N., C. M. Klinger, R. A. Rachubinski, and A. J. Simmonds, 2016 A systematic cell-based analysis of localization of predicted Drosophila peroxisomal proteins. Traffic 17: 536–553.

Barry, W. E., and C. S. Thummel, 2016 The Drosophila HNF4 nuclear receptor promotes glucose-stimulated insulin secretion and mitochondrial function in adults. Elife 5: e11183.

Bartlett, K., and S. Eaton, 2004 Mitochondrial beta-oxidation. Eur. J. Biochem. 271: 462–469.

Blad, C. C., C. Tang, and S. Offermanns, 2012 G protein-coupled receptors for energy metabolites as new therapeutic targets. Nat. Rev. Drug Discov. 11: 603–619.

Brown, M. S., and J. L. Goldstein, 1997 The SREBP pathway: regulation of cholesterol metabolism by proteolysis of a membrane-bound transcription factor. Cell 89: 331–340.

Buszczak, M., S. Paterno, D. Lighthouse, J. Bachman, J. Planck *et al.*, 2007 The carnegie protein trap library: a versatile tool for Drosophila developmental studies. Genetics 175: 1505–1531.

Canavoso, L. E., Z. E. Jouni, K. J. Karnas, J. E. Pennington, and M. A. Wells, 2001 Fat metabolism in insects. Annu. Rev. Nutr. 21: 23–46.

Chandel, N. S., H. Jasper, T. T. Ho, and E. Passegue, 2016 Metabolic regulation of stem cell function in tissue homeostasis and organismal ageing. Nat. Cell Biol. 18: 823–832.

Chatterjee, D., S. D. Katewa, Y. Qi, S. A. Jackson, P. Kapahi *et al.*, 2014 Control of metabolic adaptation to fasting by dILP6-induced insulin signaling in Drosophila oenocytes. Proc. Natl. Acad. Sci. USA 111: 17959–17964.

Dawaliby, R., C. Trubbia, C. Delporte, M. Masureel, P. Van Antwerpen *et al.*, 2016 Allosteric regulation of G protein-coupled receptor activity by phospholipids. Nat. Chem. Biol. 12: 35–39.

Deng, T., J. L. Lyon, S. Bergin, M. A. Caligiuri, and W. A. Hsueh, 2016 Obesity, inflammation, and cancer. Annu. Rev. Pathol. Mech. Dis. 11: 421–449.

Dijkman, P. M., and A. Watts, 2015 Lipid modulation of early G protein-coupled receptor signalling events. Biochim. Biophys. Acta 1848: 2889–2897.

Dobrosotskaya, I. Y., A. C. Seegmiller, M. S. Brown, J. L. Goldstein, and R. B. Rawson, 2002 Regulation of SREBP processing and membrane lipid production by phospholipids in Drosophila. Science 296: 879–883.

Drummond-Barbosa, D., and A. C. Spradling, 2001 Stem cells and their progeny respond to nutritional changes during Drosophila oogenesis. Dev. Biol. 231: 265–278.

Eden, E., R. Navon, I. Steinfeld, D. Lipson, and Z. Yakhini, 2009 GOrilla: a tool for discovery and visualization of enriched GO terms in ranked gene lists. BMC Bioinformatics 10: 48.

Ellis, J. M., L. O. Li, P. C. Wu, T. R. Koves, O. Ilkayeva *et al.*, 2010 Adipose acyl-CoA synthetase-1 directs fatty acids toward beta-oxidation and is required for cold thermogenesis. Cell Metab. 12: 53–64.

Fasshauer, M., and M. Bluher, 2015 Adipokines in health and disease. Trends Pharmacol. Sci. 36: 461–470.
Faust, J. E., A. Verma, C. Peng, and J. A. McNew, 2012 An inventory of peroxisomal proteins and pathways in Drosophila melanogaster. Traffic 13: 1378–1392.
Fergestad, T., B. Bostwick, and B. Ganetzky, 2006 Metabolic disruption in Drosophila bang-sensitive seizure mutants. Genetics 173: 1357–1364.
Forman, B. M., 2005 Are those phospholipids in your pocket? Cell Metab. 1: 153–155.
Garrido, D., T. Rubin, M. Poidevin, B. Maroni, A. Le Rouzic *et al.*, 2015 Fatty acid synthase cooperates with glyoxalase 1 to protect against sugar toxicity. PLoS Genet. 11: e1004995.
Green, E. W., G. Fedele, F. Giorgini, and C. P. Kyriacou, 2014 A Drosophila RNAi collection is subject to dominant phenotypic effects. Nat. Methods 11: 222–223.
Grell, E. H., 1976 Genetic analysis of aspartate aminotransferase isozymes from hybrids between Drosophila melanogaster and Drosophila simulans and mutagen-induced isozyme variants. Genetics 83: 753–764.
Gutierrez, E., D. Wiggins, B. Fielding, and A. P. Gould, 2007 Specialized hepatocyte-like cells regulate Drosophila lipid metabolism. Nature 445: 275–280.
Hayward, D. C., S. J. Delaney, H. D. Campbell, A. Ghysen, S. Benzer *et al.*, 1993 The sluggish-A gene of Drosophila melanogaster is expressed in the nervous system and encodes proline oxidase, a mitochondrial enzyme involved in glutamate biosynthesis. Proc. Natl. Acad. Sci. USA 90: 2979–2983.
Herr, D. R., H. Fyrst, V. Phan, K. Heinecke, R. Georges *et al.*, 2003 Sply regulation of sphingolipid signaling molecules is essential for Drosophila development. Development 130: 2443–2453.
Huang, X., J. T. Warren, and L. I. Gilbert, 2008 New players in the regulation of ecdysone biosynthesis. J. Genet. Genomics 35: 1–10.
Huang da, W., B. T. Sherman, and R. A. Lempicki, 2009 Systematic and integrative analysis of large gene lists using DAVID bioinformatics resources. Nat. Protoc. 4: 44–57.
Janke, R., A. E. Dodson, and J. Rine, 2015 Metabolism and epigenetics. Annu. Rev. Cell Dev. Biol. 31: 473–496.
Johnson, M. B., and F. M. Butterworth, 1985 Maturation and aging of adult fat body and oenocytes in Drosophila as revealed by light microscopic morphometry. J. Morphol. 184: 51–59.
Jones, H. E., J. L. Harwood, I. D. Bowen, and G. Griffiths, 1992 Lipid composition of subcellular membranes from larvae and prepupae of Drosophila melanogaster. Lipids 27: 984–987.
Kanehisa, M., Y. Sato, M. Kawashima, M. Furumichi, and M. Tanabe, 2016 KEGG as a reference resource for gene and protein annotation. Nucleic Acids Res. 44: D457–D462.
Kim, J., H. Bang, S. Ko, I. Jung, H. Hong *et al.*, 2008 Drosophila ia2 modulates secretion of insulin-like peptide. Comp. Biochem. Physiol. A Mol. Integr. Physiol. 151: 180–184.
Kühnlein, R. P., 2012 Lipid droplet-based storage fat metabolism in Drosophila: thematic review series: lipid droplet synthesis and metabolism: from yeast to man. J. Lipid Res. 53: 1430–1436.
Laws, K. M., and D. Drummond-Barbosa, 2015 Genetic mosaic analysis of stem cell lineages in the Drosophila ovary. Methods Mol. Biol. 1328: 57–72.
Laws, K. M., and D. Drummond-Barbosa, 2016 AMP-activated protein kinase has diet-dependent and -independent roles in Drosophila oogenesis. Dev. Biol. 420: 90–99.
Laws, K. M., L. L. Sampson, and D. Drummond-Barbosa, 2015 Insulin-independent role of adiponectin receptor signaling in Drosophila germline stem cell maintenance. Dev. Biol. 399: 226–236.
Li, J. Y., N. Paragas, R. M. Ned, A. Qiu, M. Viltard *et al.*, 2009 Scara5 is a ferritin receptor mediating non-transferrin iron delivery. Dev. Cell 16: 35–46.
Linder, M. C., L. Wooten, P. Cerveza, S. Cotton, R. Shulze *et al.*, 1998 Copper transport. Am. J. Clin. Nutr. 67: 965S–971S.
Lowe, N., J. S. Rees, J. Roote, E. Ryder, I. M. Armean *et al.*, 2014 Analysis of the expression patterns, subcellular localisations and interaction partners of Drosophila proteins using a pigP protein trap library. Development 141: 3994–4005.
MacMillan, H. A., and B. N. Hughson, 2014 A high-throughput method of hemolymph extraction from adult Drosophila without anesthesia. J. Insect Physiol. 63: 27–31.
Martinez-Outschoorn, U., F. Sotgia, and M. P. Lisanti, 2014 Tumor microenvironment and metabolic synergy in breast cancers: critical importance of mitochondrial fuels and function. Semin. Oncol. 41: 195–216.
McGuire, S. E., P. T. Le, A. J. Osborn, K. Matsumoto, and R. L. Davis, 2003 Spatiotemporal rescue of memory dysfunction in Drosophila. Science 302: 1765–1768.
Menzies, K. J., H. Zhang, E. Katsyuba, and J. Auwerx, 2016 Protein acetylation in metabolism-metabolites and cofactors. Nat. Rev. Endocrinol. 12: 43–60.
Montal, E. D., R. Dewi, K. Bhalla, L. Ou, B. J. Hwang *et al.*, 2015 PEPCK coordinates the regulation of central carbon metabolism to promote cancer cell growth. Mol. Cell 60: 571–583.
Moraes, A. S., B. de Campos Vidal, A. M. Guaraldo, and M. L. Mello, 2005 Chromatin supraorganization and extensibility in mouse hepatocytes following starvation and refeeding. Cytometry A 63: 94–107.
Moser, D., L. Johnson, and C. Y. Lee, 1980 Multiple forms of Drosophila hexokinase. Purification, biochemical and immunological characterization. J. Biol. Chem. 255: 4673–4679.
Newman, J. C., and E. Verdin, 2014 Ketone bodies as signaling metabolites. Trends Endocrinol. Metab. 25: 42–52.
Nichol, H., and M. Locke, 1990 The localization of ferritin in insects. Tissue Cell 22: 767–777.
Nieman, K. M., H. A. Kenny, C. V. Penicka, A. Ladanyi, R. Buell-Gutbrod *et al.*, 2011 Adipocytes promote ovarian cancer metastasis and provide energy for rapid tumor growth. Nat. Med. 17: 1498–1503.
Ohno, C. K., and M. Petkovich, 1993 FTZ-F1 beta, a novel member of the Drosophila nuclear receptor family. Mech. Dev. 40: 13–24.
Palm, W., J. L. Sampaio, M. Brankatschk, M. Carvalho, A. Mahmoud *et al.*, 2012 Lipoproteins in Drosophila melanogaster–assembly, function, and influence on tissue lipid composition. PLoS Genet. 8: e1002828.
Parker, K., J. Maxson, A. Mooney, and E. A. Wiley, 2007 Class I histone deacetylase Thd1p promotes global chromatin condensation in Tetrahymena thermophila. Eukaryot. Cell 6: 1913–1924.
Parra-Peralbo, E., and J. Culi, 2011 Drosophila lipophorin receptors mediate the uptake of neutral lipids in oocytes and imaginal disc cells by an endocytosis-independent mechanism. PLoS Genet. 7: e1001297.
Pascual, A., M. Chaminade, and T. Preat, 2005 Ethanolamine kinase controls neuroblast divisions in Drosophila mushroom bodies. Dev. Biol. 280: 177–186.
Pavlidis, P., M. Ramaswami, and M. A. Tanouye, 1994 The Drosophila easily shocked gene: a mutation in a phospholipid synthetic pathway causes seizure, neuronal failure, and paralysis. Cell 79: 23–33.
Pietrocola, F., L. Galluzzi, J. M. Bravo-San Pedro, F. Madeo, and G. Kroemer, 2015 Acetyl coenzyme A: a central metabolite and second messenger. Cell Metab. 21: 805–821.
Rosen, E. D., and B. M. Spiegelman, 2014 What we talk about when we talk about fat. Cell 156: 20–44.
Ross, P. L., Y. N. Huang, J. N. Marchese, B. Williamson, K. Parker *et al.*, 2004 Multiplexed protein quantification in *Saccharomyces*

cerevisiae using amine-reactive isobaric tagging reagents. Mol. Cell. Proteomics 3: 1154–1169.

Schwartz, M., T. J. Kelly, R. B. Imberski, and E. C. Rubenstein, 1985 The effects of nutrition and methoprene treatment on ovarian ecdysteroid synthesis in Drosophila melanogaster. J. Insect Physiol. 31: 947–957.

Seegmiller, A. C., I. Dobrosotskaya, J. L. Goldstein, Y. K. Ho, M. S. Brown *et al.*, 2002 The SREBP pathway in Drosophila: regulation by palmitate, not sterols. Dev. Cell 2: 229–238.

Shyh-Chang, N., G. Q. Daley, and L. C. Cantley, 2013 Stem cell metabolism in tissue development and aging. Development 140: 2535–2547.

Spradling, A., 1993 Developmental genetics of oogenesis, pp. 1–70 in *The Development of Drosophila Melanogaster*, edited by M. Bate. Cold Spring Harbor Laboratory Press, Cold Spring Harbor, NY.

Sun, J., and A. C. Spradling, 2012 NR5A nuclear receptor Hr39 controls three-cell secretory unit formation in Drosophila female reproductive glands. Curr. Biol. 22: 862–871.

Tang, X., and B. Zhou, 2013a Ferritin is the key to dietary iron absorption and tissue iron detoxification in Drosophila melanogaster. FASEB J. 27: 288–298.

Tang, X., and B. Zhou, 2013b Iron homeostasis in insects: insights from Drosophila studies. IUBMB Life 65: 863–872.

Tennessen, J. M., K. D. Baker, G. Lam, J. Evans, and C. S. Thummel, 2011 The Drosophila estrogen-related receptor directs a metabolic switch that supports developmental growth. Cell Metab. 13: 139–148.

Tennessen, J. M., W. E. Barry, J. Cox, and C. S. Thummel, 2014 Methods for studying metabolism in Drosophila. Methods 68: 105–115.

Todorich, B., X. Zhang, B. Slagle-Webb, W. E. Seaman, and J. R. Connor, 2008 Tim-2 is the receptor for H-ferritin on oligodendrocytes. J. Neurochem. 107: 1495–1505.

Vance, J. E., and G. Tasseva, 2013 Formation and function of phosphatidylserine and phosphatidylethanolamine in mammalian cells. Biochim. Biophys. Acta 1831: 543–554.

Vander Heiden, M. G., L. C. Cantley, and C. B. Thompson, 2009 Understanding the Warburg effect: the metabolic requirements of cell proliferation. Science 324: 1029–1033.

Wang, W., M. A. Knovich, L. G. Coffman, F. M. Torti, and S. V. Torti, 2010 Serum ferritin: past, present and future. Biochim. Biophys. Acta 1800: 760–769.

Wellen, K. E., G. Hatzivassiliou, U. M. Sachdeva, T. V. Bui, J. R. Cross *et al.*, 2009 ATP-citrate lyase links cellular metabolism to histone acetylation. Science 324: 1076–1080.

Wellner, N., T. A. Diep, C. Janfelt, and H. S. Hansen, 2013 N-acylation of phosphatidylethanolamine and its biological functions in mammals. Biochim. Biophys. Acta 1831: 652–662.

Whitaker-Menezes, D., U. E. Martinez-Outschoorn, Z. Lin, A. Ertel, N. Flomenberg *et al.*, 2011 Evidence for a stromal-epithelial "lactate shuttle" in human tumors: MCT4 is a marker of oxidative stress in cancer-associated fibroblasts. Cell Cycle 10: 1772–1783.

Yazawa, T., Y. Imamichi, K. Miyamoto, M. R. Khan, J. Uwada *et al.*, 2015 Regulation of steroidogenesis, development, and cell differentiation by steroidogenic factor-1 and liver receptor homolog-1. Zoolog. Sci. 32: 323–330.

Zhao, S., A. Torres, R. A. Henry, S. Trefely, M. Wallace *et al.*, 2016 ATP-citrate lyase controls a glucose-to-acetate metabolic switch. Cell Rep. 17: 1037–1052.

Communicating editor: D. I. Greenstein